

Spectrum of pore types and networks in mudrocks and a descriptive classification for matrix-related mudrock pores

Robert G. Loucks, Robert M. Reed, Stephen C. Ruppel, and Ursula Hammes

ABSTRACT

Matrix-related pore networks in mudrocks are composed of nanometer- to micrometer-size pores. In shale-gas systems, these pores, along with natural fractures, form the flow-path (permeability) network that allows flow of gas from the mudrock to induced fractures during production. A pore classification consisting of three major matrix-related pore types is presented that can be used to quantify matrix-related pores and relate them to pore networks. Two pore types are associated with the mineral matrix; the third pore type is associated with organic matter (OM). Fracture pores are not controlled by individual matrix particles and are not part of this classification. Pores associated with mineral particles can be subdivided into interparticle (interP) pores that are found between particles and crystals and intraparticle (intraP) pores that are located within particles. Organic-matter pores are intraP pores located within OM. Interparticle mineral pores have a higher probability of being part of an effective pore network than intraP mineral pores because they are more likely to be interconnected. Although they are intraP, OM pores are also likely to be part of an interconnected network because of the interconnectivity of OM particles.

In unlithified near-surface muds, pores consist of interP and intraP pores, and as the muds are buried, they compact and lithify. During the compaction process, a large number of interP and intraP pores are destroyed, especially in ductile grain-rich muds. Compaction can decrease the pore volume up to

AUTHORS

ROBERT G. LOUCKS ~ *Bureau of Economic Geology, Jackson School of Geosciences, University of Texas at Austin, University Station, Box X, Austin, Texas; bob.loucks@beg.utexas.edu*

Robert G. Loucks is a senior research scientist at the Bureau of Economic Geology. He received his B.A. degree from the State University of New York at Binghamton in 1967 and his Ph.D. from the University of Texas at Austin in 1976. His general research interests include carbonate and siliciclastic sequence stratigraphy, depositional systems, diagenesis, and reservoir characterization. His present research includes pore networks in carbonates, sandstones, and mudrocks; evaporite and carbonate paleokarst; deep to ultradeep reservoirs in the Gulf of Mexico; and shale-gas systems.

ROBERT M. REED ~ *Bureau of Economic Geology, Jackson School of Geosciences, University of Texas at Austin, University Station, Box X, Austin, Texas; rob.reed@beg.utexas.edu*

Rob M. Reed is a research scientist associate at the Bureau of Economic Geology. He received his B.S. degree and his Ph.D. in geologic sciences from the University of Texas at Austin and his M.S. degree in geology from the University of Massachusetts. His current research focuses on various aspects of the microstructure of rocks.

STEPHEN C. RUPPEL ~ *Bureau of Economic Geology, Jackson School of Geosciences, University of Texas at Austin, University Station, Box X, Austin, Texas; stephen.ruppel@beg.utexas.edu*

Stephen C. Ruppel is a senior research scientist at the Bureau of Economic Geology in Austin, where he specializes in sedimentologic characterization of carbonate and mudrock successions and is currently director of the Mudrock Systems Research Laboratory. Before coming to the Bureau in 1981, he worked at McGill University in Montreal and Chevron Oil Company in New Orleans. He received his Ph.D. from the University of Tennessee and his B.S. and M.S. degrees from the University of Illinois and University of Florida, respectively. His current research is focused on integrating sedimentologic, geochemical, and stratigraphic data from outcropping and subsurface Paleozoic and

Copyright ©2012. The American Association of Petroleum Geologists. All rights reserved.

Manuscript received May 16, 2011; provisional acceptance July 25, 2011; revised manuscript received August 2, 2011; final acceptance August 17, 2011.

DOI:10.1306/08171111061

Mesozoic carbonate and shale successions to develop process and response models of deposition and diagenesis.

URSULA HAMMES ~ *Bureau of Economic Geology, Jackson School of Geosciences, University of Texas at Austin, University Station, Box X, Austin, Texas;*
ursula.hammes@beg.utexas.edu

Ursula Hammes obtained her diploma in geology from the University of Erlangen in Germany in 1987 and her Ph.D. from the University of Colorado at Boulder in 1992. She spent 10 yr working as a consultant, performing postdoctoral research at the Bureau of Economic Geology and as an exploration geologist in the industry. She joined the Bureau of Economic Geology in 2001 as a research associate. Her main research focus is in clastic and carbonate sequence stratigraphy, depositional systems, and carbonate and clastic diagenesis. Her recent research objective is in shale-gas systems in Texas and Germany.

ACKNOWLEDGEMENTS

This research was funded by the Mudrock Systems Research Laboratory and the State of Texas Advanced Resource Recovery (STARR) Project at the Bureau of Economic Geology. Industry members include Anadarko, BP, Chesapeake, Chevron, Cima, Cimarex, ConocoPhillips, Cypress, Devon, Encana, EOG Resources, EXCO Resources, Husky, Marathon, Pangaea, Penn Virginia, Penn West, Pioneer, Shell, StatOil, Texas American Resources, The Unconventionals, U.S. EnerCorp, Valence, and YPF (Yacimientos Petroliferos Fiscales). Editing was provided by Lana Dieterich, Bureau of Economic Geology. The authors acknowledge reviews by David Awwiller, Shirley Dutton, Terri Olson, and Arthur Trevena. Ruari Day-Stirrat provided an ion-milled sample from the Ursa Basin in the Gulf of Mexico. Publication was authorized by the director of Bureau of Economic Geology, Jackson School of Geosciences, University of Texas at Austin. The AAPG Editor thanks the following reviewers for their work on this paper: David N. Awwiller, Terrilyn M. Olson, and Arthur Trevena.

88% by several kilometers of burial. At the onset of hydrocarbon thermal maturation, OM pores are created in kerogen. At depth, dissolution of chemically unstable particles can create additional moldic intraP pores.

INTRODUCTION

Nanometer- to micrometer-size connected matrix-related pores form flow networks, along with fractures where present, that contribute to the natural permeability pathways for gas flow in unconventional mudrock reservoirs (the term “mudrock” is used to include mudstones and shales) (Javadpour, 2009; Curtis et al., 2010). Research during the last several years has identified a variety of pore types in these mudrocks (i.e., Davies et al., 1991; Desbois et al., 2009; Loucks et al., 2009, 2010; Curtis et al., 2010; Diaz et al., 2010; Milner et al., 2010; Passey et al., 2010; Schieber, 2010; Sisk et al., 2010; Lu et al., 2011; Slatt and O’Neal, 2011). We propose a simple, relatively objective, descriptive approach to grouping mudrock matrix-related pores into three basic categories on the basis of their relationships to particles (Figure 1). Pore types include interparticle (interP) mineral pores, intraparticle (intraP) mineral pores, and intraP organic-matter (OM) pores. This type of pore classification is consistent with schemes of pore subdivisions used in conventional sandstone (i.e., Pittman, 1979) and carbonate (i.e., Choquette and Pray, 1970) reservoir systems. Although descriptive, it provides a first step in relating pores to reservoir properties. For example, type, size, and arrangement of pores affect storage and calculations of hydrocarbons in place (i.e., Ambrose et al., 2010) as well as sealing capacity (Dawson and Almon, 2002; Dewhurst et al., 2002; Schieber, 2010). Also, differences in the origins and distribution of pore types have been shown to have different effects on permeability and wettability (i.e., McCreesh et al., 1991; Passey et al., 2010). These three categories of pores can be plotted on a ternary diagram to compare different scales of sampling, such as different areas of a scanning electron microscope (SEM) sample, different intervals of an individual shale play, or summary comparisons of different shale plays in different basins.

The major goals of this article are to document in a simple and systematic manner the wide spectrum of matrix-related pores that exist in mudrocks and classify these pores on the basis of basic descriptive attributes. Specific objectives are to (1) present a pore classification that summarizes the spectrum of pore types seen in mudrock reservoirs and that also captures some important petrophysical properties of the pores;

(2) introduce a ternary classification that allows comparison of mudrocks that contain matrix-related pores; (3) compare pores within unlithified and shallow muds with pores within ancient, more deeply buried lithified mudrocks; and (4) discuss how different pore types contribute to effective matrix-flow pathways in mudrocks.

DATA AND METHODS

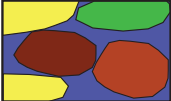
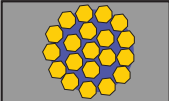


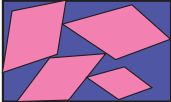
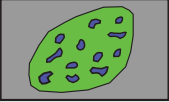
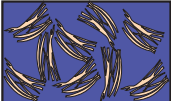
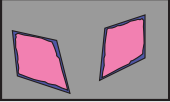
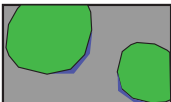
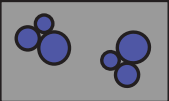

Data for this investigation of pore types in mudrocks come from core and outcrop samples collected from a variety of formations. Many of the data were generated by the Mudrock Systems Research Laboratory at the Bureau of Economic Geology, Jackson School of Geosciences, University of Texas at Austin. Some data are from published studies that contain SEM photomicrographs of mudrock pores. Table 1 presents a summary of data showing the age, unit name, general location, pore types according to present classification, and source of data. The 26 geologic units included in this survey range in age from Cambrian to Pliocene–Pleistocene, in depth from outcrop to 15,950 ft (4752 m), and in maturity from less than 0.5 to 3.17% vitrinite reflectance (R_o).

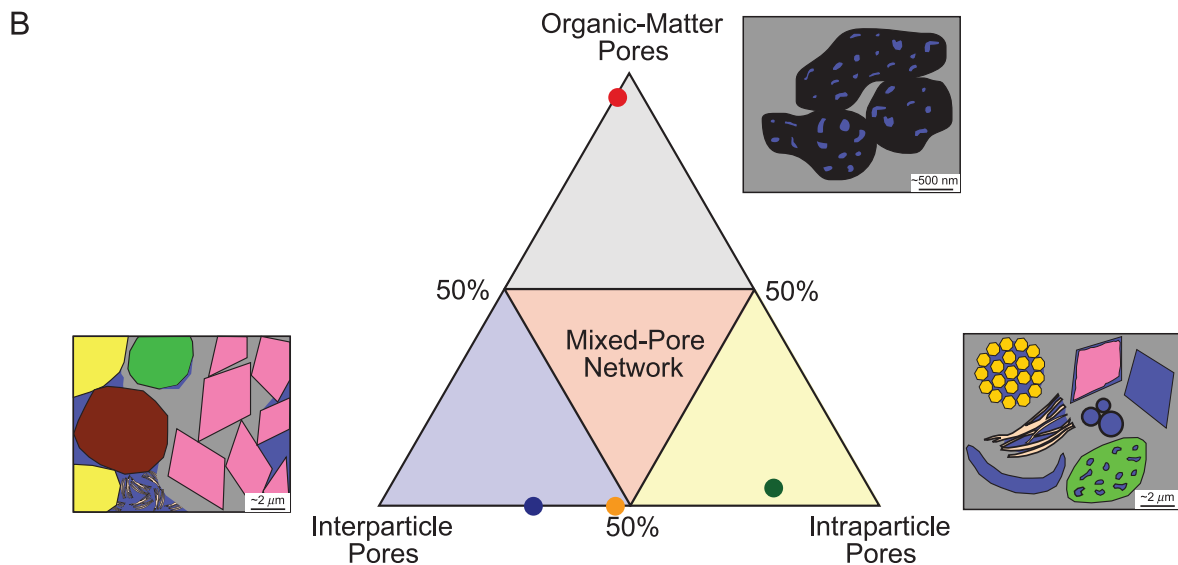
As pointed out by Loucks et al. (2009), most of the small pores in mudrocks are generally smaller than a few micrometers in diameter and cannot be seen using light microscopy. These workers also noted that polished thin sections produced surface topographic irregularities (their figure 3) because of differential hardness of components, making thin sections inadequate for pore identification using SEM-based imaging techniques. Pittman (1992) also noted that grains are plucked out during thin-section preparation, producing artifact pores. Rock chips have a tendency to produce a pull-out of grains (grain plucking) that may be misidentified as pores, and this dilemma gives a low confidence level of correct identification of artifacts from actual pores. Some authors (i.e., Milner et al., 2010) disagreed with the inadequacies of rock chips, but detailed work by the present authors has substantiated abundant pull-out artifacts, as has the work by Sondergeld et al. (2010).

Hildenbrand and Urai (2003) used Wood's metal injection technique to create pore casts in mudrocks. They were able to image a pore cast as small as 40 nm in diameter and showed larger pores connected by smaller pore throats (their figure 11). Theirs is an interesting and informative technique and should be considered in the study of mudrock pore networks. However, we think that our method (described herein) displays pores more clearly. Methods that indirectly attempt analysis of pore structures in mudrocks also exist, such as by conducting high-pressure CH_4 isotherm analysis (Ross and Bustin, 2009). These techniques were not used in this study.

Our samples were all prepared using ion-milling techniques (Reed and Loucks, 2007; Loucks et al., 2009). The technique is similar to a common method for preparation of electron-transparent transmission electron microscope samples (e.g., Hover et al., 1996), although the milling is confined to one surface instead of two. Argon (Ar)-ion-beam milling produces surfaces showing only minor topographic variations unrelated to differences in hardness of the sample but, rather, to slight variations in the path of the Ar-ion beam. Tomutsa et al. (2007) promoted using this ion-milling technique to image pore systems in diatomite and chalk. These flat surfaces allow the quantification of types and number of pores in two dimensions. Pores viewed within three-dimensional (3-D) rock chips cannot be quantified because of the irregular surface and associated pull-outs. A limitation of using Ar-ion-milled samples is the inherently small viewing area provided by this technique. The milled area measures only approximately 1.5×0.5 mm. Although this area is small, relative to the nanometer to micrometer size of pores in mudstones, many pores can nonetheless be observed.

Artifacts associated with sample preparation and Ar-ion milling exists, but they are easy to recognize. Samples with clay-rich matrix and large clay particles can desiccate and produce shrinkage cracks (Figure 2A–C) on drying. The most common artifacts associated with ion milling are (1) redeposition of milled material within some pores (Figure 2D) and (2) curtaining (Figure 2E, F). Curtaining, which is typically expressed as flaring structures associated

A		Organic-Matter Pores	Fracture Pores
Mineral Matrix Pores Pores between or within mineral particles		Pores within organic matter	Pores not controlled by individual particles
Interparticle Pores	Intraparticle Pores	Organic-Matter Pores	Fracture Pores
			
Pores between grains	Intercrystalline pores within pyrite framboids		
			
Pores between crystals	Pores within peloids or pellets		
			
Pores between clay platelets	Dissolution-rim pores		
			
Pores at the edge of rigid grains	Pores within fossil bodies		
			
	Moldic pores after a crystal		
	Moldic pores after a fossil		



with minor relief, is primarily a minor annoyance in photomicrographs; it is easily identified and presents no major problems for pore identification. Redeposition of milled material is a more serious problem, if not recognized. Although not documented, this process could completely fill some of the smaller pore population; the redeposited material can be recognized, however, in backscatter by contrast in density. Redeposited material appears as anomalous lighter colored areas around the edges of pores; this material commonly fills the upflow part of larger pores (Figure 2D).

Ion-milled samples were imaged on several types of SEMs. Samples were examined using two different field-emission SEMs. One was a Zeiss Supra 40 VP and the other was an FEI Nova NanoSEM 430. Both systems are at the University of Texas at Austin. Use of these field-emission SEMs equipped with in-lens secondary electron (SE) detectors provides greatly increased detail of nanometer-scale features. Lower accelerating voltages (1–10 kV) were typically used on these systems to prevent beam damage of the sample. Working distances were 3 to 7 mm.

Secondary electron images were acquired for documenting topographic variation, and backscattered secondary electron (BSE) images were acquired for delineating compositional variation. Energy dispersive spectroscopy analyses of specific grains were also conducted for mineral identification. These analyses and images provided the basic data for lithologic determination and types and locations of pores within the sample.

Several publications (Table 1) have provided excellent photographs of mudrock pores acquired by SEM imaging. Nearly all the samples, including

those from the literature, were prepared using the ion-milling technique. These published data provided an additional range of sample age and regional extent to our own data. Other authors have used different terminologies to name and classify pore types. Tables 1 and 2 compare their terminology with the terminology used in this article.

The upper pore-size range in mudrocks is generally less than a few micrometers, with most pores being less than 1 μm . Chalmers et al. (2009) recommended that geoscientists working on mudrocks use the pore-size terminology of the International Union of Pure and Applied Chemistry, as developed by Rouquerol et al. (1994). Micropores, as defined by Rouquerol et al. (1994), have widths less than 2 nm, mesopores have widths between 2 and 50 nm, and macropores have widths greater than 50 nm. In this classification, nearly all mudrock pores would be grouped with larger pores in carbonates and sandstones as macropores (Figure 3). Although the pore-size classification of Rouquerol et al. (1994) may be appropriate for chemical products, such as describing membranes, it is insufficient for reservoir systems. Choquette and Pray (1970) provided a useful pore classification for carbonate rocks, within which they provided size modifiers. They defined micropores as being less than 62.5 μm , mesopores as being between 62.5 μm and 4 mm, and megapores as being between 4 and 256 mm. These authors included no subdivisions of pores smaller than 62.5 μm .

Because many mudrock pores commonly range from a few nanometers to several micrometers in diameter, it would be useful to have well-defined names for pores in this size range and for pores smaller than this size range. We propose the terms

Figure 1. Pore type classes. (A) Spectrum of pore types occurring within mudrocks. General pore types include interparticle and intraparticle pores associated with mineral matrix, organic-matter pores associated with organic matter, and fracture pores that crosscut matrix and grains. Examples of common pore types are presented but are not meant to indicate formal subtypes or terminology. Fracture pores are presented in this figure only to emphasize their importance. However, they are not considered matrix-related pores and are not part of the matrix-related classification presented in this study. (B) The mudrock pore classification ternary diagram was modified from Loucks et al. (2010). If a pore network is dominated by 50% or more of one pore type, it assumes the name of that pore type. If no one pore type dominates, then it is a mixed-pore network. Examples of pore networks (shown in Figures 5A, 13) from the Barnett Shale (red circle), Bossier Shale (green circle), Pearsall Formation (blue circle), and a Pliocene–Pleistocene mudstone (orange circle) are plotted. The proportion of pore types for the Barnett, Bossier, and Pearsall was derived by point counting 2000 points and for the Pliocene–Pleistocene by point counting 1000 points.

Table 1. Data Used to Develop Pore Types*

Age	Unit Name	General Location	Pore Type (this article)**	Pore Type as Described by Author	Source [†]
Pliocene–Pleistocene		Nankai accretionary prism, offshore Japan	InterP dominant and intraP present	Intergranular pores (authors' figure 11)	Milliken and Reed (2010)
Pliocene–Pleistocene		Ursa Basin Gulf of Mexico	InterP dominant and intraP present	No data provided	Day-Stirrat et al. (2010b)
Oligocene	Boom Clay	Mol, Belgium	InterP and intraP	Three types: Type I elongated pores between similarly oriented clay sheets (<100 nm), type II crescent-shaped pores in saddle reefs of folded sheet of clay (100 nm–1 μ m), and type III large, jagged pores surrounding clast grains (>1 μ m) (authors' figures 3, 4)	Desbois et al. (2009)
Eocene	Wilcox Group	West Baton Rouge Parish, Louisiana	InterP and intraP	Type I pores are aligned parallel to clay-mineral cleavage (authors' figure 10A, B), type II pores are bedding-parallel cleavage cracks through several grains (authors' figure 10C), type III wedge-shaped pores are voids at terminations of stacked clay platelets (authors' figure 11A), type IV pores are at face-edge mineral contacts (authors' figure 11B), type V pores occur at interfaces between clays and detrital grains (authors' figure 11C), and type VI microfractures occur within rigid grains (authors' figure 11C)	Kwon et al. (2004)
Late Cretaceous	Tuscaloosa Group	Mississippi	IntraP and OM	Pores within pyrite framboids (authors' figure 9A), inorganic matter (authors' figure 9B), fluid-inclusions pores (authors' figure 9C), and pores in dissolved TiO ₂ grain (authors' figure 9D)	Lu et al. (2011)
Late Cretaceous	Eagle Ford Formation	South Texas shelf	InterP and intraP dominant, lesser OM		Loucks et al. (2010) and MSRL study
Late Cretaceous	Eagle Ford Formation	South Texas shelf	IntraP and OM	Phyllosilicate and organophyllic pores (authors' figure 8)	Curtis et al. (2010)
Early Cretaceous	Mancos Shale	Book Cliffs, Utah	InterP and intraP	Phyllosilicate framework (author's figure 4A–C)	Schieber (2010)
Early Cretaceous	Pearsall Formation	South Texas Maverick Basin	InterP and intraP dominant, lesser OM		Loucks et al. (2010) and MSRL study
Late Jurassic	Kimmeridge Clay	Europe	OM dominant	Organophyllic pores (authors' figure 8)	Curtis et al. (2010)
Late Jurassic	Haynesville Formation	East Texas Basin	InterP and intraP with minor OM		Loucks et al. (2010) and MSRL study

Late Jurassic	Haynesville Formation	East Texas Basin	InterP and intraP with minor OM	Matrix intercrystalline and organic pores (authors' figure 1A–C) and intraP pore (authors' figure 3)	Milner et al. (2010)
Late Jurassic	Haynesville Formation	East Texas Basin	InterP and intraP with minor OM	Phyllosilicate pores (authors' figures 8, 10, 16, 17)	Curtis et al. (2010)
Late Jurassic	Bossier Shale	East Texas Basin	InterP and intraP with minor OM		Loucks et al. (2010) and MSRL study
Pennsylvanian	Atoka Formation	Permian Basin	Rare interP and intraP, no OM		Loucks et al. (2010) and MSRL study
Carboniferous Mississippian	Barnett Shale	Germany Fort Worth Basin and Permian Basin	InterP, intraP, and OM OM dominant with intraP in pyrite framboids		MSRL study Loucks et al. (2009), Loucks et al. (2010), and MSRL study
Mississippian	Barnett Shale	Forth Worth Basin	OM dominant	Organophyllic pores (authors' figure 8)	Curtis et al. (2010)
Mississippian	Barnett Shale	Fort Worth Basin	OM dominant	Organic matter pores (authors' figure 2A–C)	Milner et al. (2010)
Mississippian	Barnett Shale	Fort Worth Basin	OM dominant with interP	Authors' figures 8, 14, 18, and 20	Sondergeld et al. (2010)
Mississippian	Fayetteville Shale	Arkoma Basin, Arkansas	IntraP and OM	Phyllosilicate and organophyllic pores (authors' figure 8)	Curtis et al. (2010)
Mississippian	Floyd Shale	Black Warrior Basin, Alabama	OM dominant	Organophyllic pores (authors' figure 8)	Curtis et al. (2010)
Mississippian	Floyd Shale	Black Warrior Basin, Alabama	OM and interP	Authors' figure 13	Sondergeld et al. (2010)
Mississippian/ Devonian	Barnett Shale and Woodford Shale	Texas	OM, interP, and intraP	Organic porosity, interP pores between flocculated particles, pores within pellets, and microchannels in matrix	Slatt and O'Neal (2011)
Devonian	Woodford Shale	Permian Basin	OM dominant		MSRL study
Devonian	Woodford Shale		OM dominant	Organophyllic pores (authors' figures 6 and 8)	Curtis et al. (2010)
Devonian	New Albany Shale	Illinois Basin	InterP and intraP		Loucks et al. (2010) and MSRL study
Devonian	New Albany Shale	Illinois Basin	InterP and intraP	Phyllosilicate framework (author's figures 1–3) and carbonate-dissolution pores (author's figure 5A, B)	Schieber (2010)
Devonian	Marcellus Shale	Northeast USA	OM dominant with minor intraP	Organic pores (authors' figure 2D–F) and intraparticle pores	Milner et al. (2010)
Devonian	Marcellus Shale	Northeast USA	OM dominant	Organophyllic pores (authors' figure 8)	Curtis et al. (2010)
Devonian	Geneseo Shale	New York	InterP, intraP, and OM	Phyllosilicate framework (author's figure 4D, E), carbonate dissolution pores (author's figure 5E, F), and organic matter pores (author's figure 6C–E)	Schieber (2010)
Devonian	Horn River Shale	Canada	OM dominant	Organic pores (authors' figure 1D–F)	Milner et al. (2010)
Devonian	Horn River Shale	Canada	OM dominant	Authors' figures 8, 9	Curtis et al. (2010)

Table 1. Continued

Age	Unit Name	General Location	Pore Type (this article)**	Pore Type as Described by Author	Source [†]
Devonian	Antrim Shale	Michigan Basin	IntraP	Cleavage pores within mica (authors' figure 3A)	Hover et al. (1996)
Devonian	Seneca Member of Onondaga Limestone	New York	IntraP	Cleavage pores within mica (authors' figure 3D)	Hover et al. (1996)
Ordovician	Maquoketa Group	Indiana	InterP, intraP, and OM	Phyllosilicate framework (author's figure 4F), carbonate dissolution pores (author's figure 5C, D), and organic matter pores (author's figure 6F)	Schieber (2010)
Cambrian	Eau Claire Formation	Indiana	InterP and intraP	Phyllosilicate framework (author's figure 4G)	Schieber (2010)

*Data include material generated by this study and material from the literature.

**InterP = interparticle; intraP = intraparticle; OM = organic matter.

[†]MSRL = samples from the Mudrock Systems Research Laboratory at the Bureau of Economic Geology, University of Texas at Austin.

“nanopore” for pores less than 1 μm (1000 nm) and greater than or equal to 1 nanometer and “picopore” for pores less than 1 nm. In our system, picropores are less than 1 nm, nanopores range from 1 nm to less than 1 μm , micropores range from 1 to less than 62.5 μm , mesopores range from 62.5 μm to less than 4 mm, and macropores are larger than 4 mm. Figure 3 compares our pore-scale scheme with that of Rouquerol et al. (1994).

MUDROCK PORE-TYPE CLASSES

Mudrock matrix-related pores range from simple to complex in shape and origin. They form by both depositional and diagenetic processes. Also, pores may show a multiple-stage origin related to deposition, compaction, cementation, and dissolution. Pores and associated pore networks are also partly a function of original matrix mineralogy (Figure 4), fabric (arrangement of grains), texture (size and sorting of grains), and OM composition.

A classification of mudrock matrix-related pores should be simple and should also incorporate, as best as possible, some inherent characteristics, such as permeability and wettability. Carbonate (i.e., Choquette and Pray, 1970; Lucia, 1999) and coarser grained siliciclastic (i.e., Pittman, 1979; Dutton and Loucks, 2010) pore classifications generally divide pores into those that occur between particles (interP) and those that occur within particles (intraP). Interparticle pores include intergranular (between grains) and intercrystalline pores (between crystals); intraP pores include moldic pores and pores in fossil cavities. Mudrocks contain pore types similar to those seen in carbonates and coarser grained siliciclastics, although much smaller in scale. However, they also contain OM pores, which have not yet been recognized in carbonate or coarser grained siliciclastic rocks. Intraparticle OM pores are created during hydrocarbon maturation (Jarvie et al., 2007; Loucks et al., 2009). Loucks et al. (2009), Ambrose et al. (2010), and Curtis et al. (2010) suggested and demonstrated that OM pores form the major connected or effective pore network in some shale-gas systems, such as the Mississippian Barnett Shale.

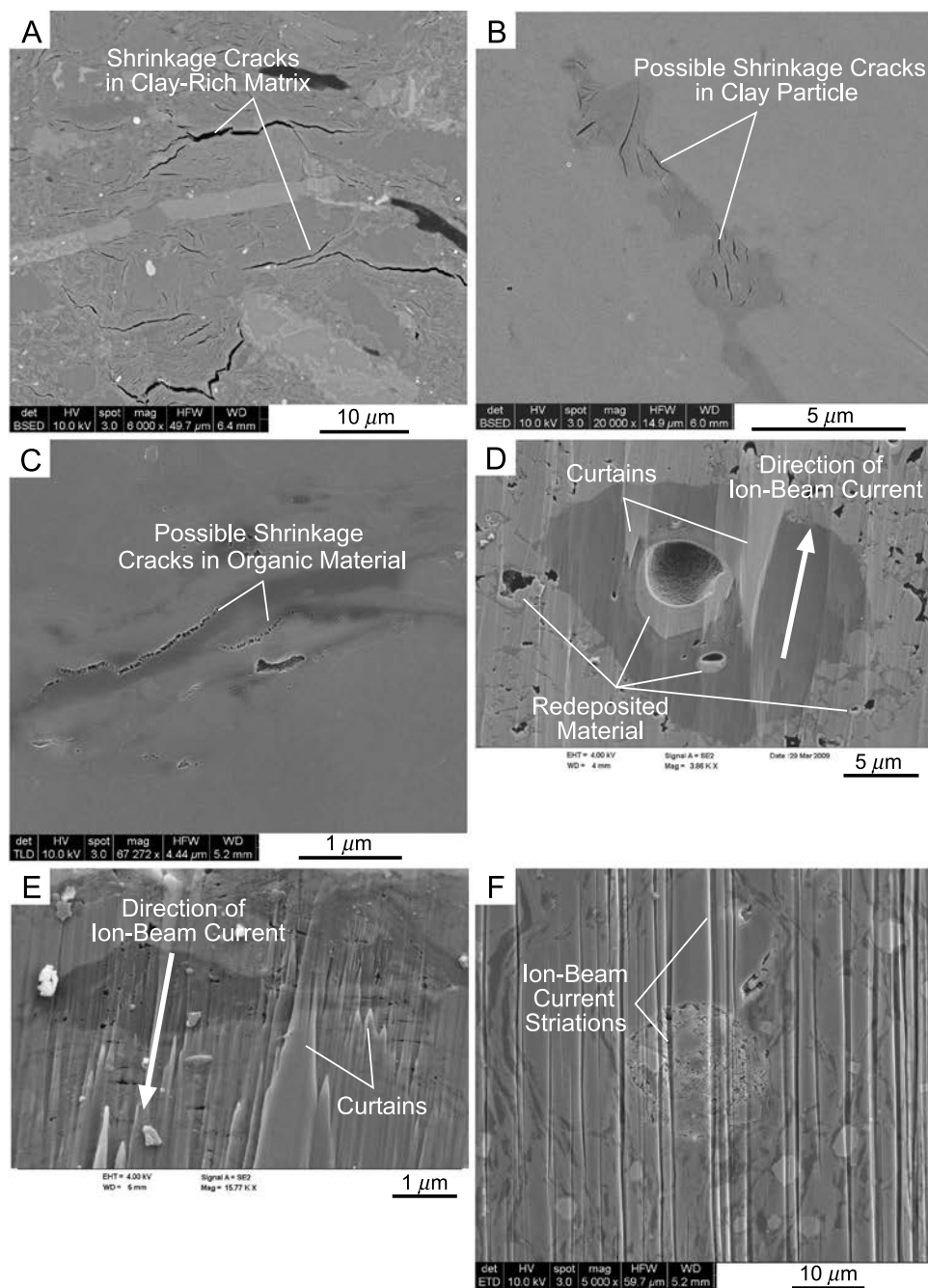


Figure 2. Common sample preparation artifacts. (A) Shrinkage of clay-rich matrix by desiccation; 10,460 ft (3188 m), Pennsylvanian Atoka interval, Andrews County, Texas. (B) Possible shrinkage cracks within clay particle by desiccation; 10,190 ft (3106 m), Pennsylvanian Atoka interval, Andrews County, Texas. (C) Possible shrinkage of organic matter showing elongated cracks with bridges across the cracks; 9700 ft (2957 m), Lower Cretaceous Pearsall Formation, Atascosa County, Texas. (D) Pores partly filled by milled material during the ion-milling process. Note that light-colored material is deposited on the sides of pores oriented toward the bottom of the photograph; 13,818 ft (4212 m), Upper Cretaceous Eagle Ford Shale, De Witt County, Texas. (E) Differential abrasion by ion beam produces curtains with sharp points oriented in an upflow direction of beam; 13,384 ft (4079 m), Upper Jurassic Bossier Shale, San Augustine County, Texas. (F) Differential relief striations formed by irregular ion-beam current; 1887 ft (575 m) Devonian New Albany Shale, Hancock County, Kentucky. det = detector; WD = working distance; mag = magnification; SE2 = secondary electron detector; TLD = through-lens detector; HV = high voltage (accelerating voltage); HFW = horizontal frame width; spot = spot size; BSED = back-scattered electron detector; EHT = electron high tension (accelerating voltage); TLD = through-lens detector.

The following sections present a simple and objective classification of mudrock matrix-related pores consisting of three basic types: (1) interP pores between grains and crystals, (2) intraP pores within mineral particles, and (3) OM pores within OM (Figure 1). A preliminary introduction to these pore types was presented by Loucks et al. (2010).

Interparticle Pores

Interparticle pores are abundant in young or shallow-buried sediments (Figure 5) and are commonly well connected, forming an effective (permeable) pore network. However, this pore network evolves with burial as overburden stress and diagenesis

Table 2. Comparison of Pore Terminology from Other Publications with Terminology Suggested by the Present Classification

Pore Types (this article)	Terminology Used by Other Authors	Reference
Interparticle	Intergranular	Milliken and Reed (2010)
	Type III: large jagged	Desbois et al. (2009)
	Phyllosilicate	Curtis et al. (2010)
	Phyllosilicate framework	Schieber (2010), Milner et al. (2010)
	Type IV: occurs at face-to-edge arrangement of clay plates; type V: pores at interfaces between clay and rigid grains	Kwon et al. (2004)
Intraparticle	Type I: elongate ; type II: crescent shape	Desbois et al. (2009)
	Phyllosilicate	Curtis et al. (2010)
	Carbonate dissolution; phyllosilicate framework	Schieber (2010), Milner et al. (2010)
	Type I: cleavage-parallel pore; type II: cracks through several grains; type III: pore at terminations of stacked clay platelets;	Kwon et al. (2004)
	type VI: intragranular fractures	
Organic matter	Intraparticle (primary in fecal pellets)	Milner et al. (2010)
	Organophyllic	Curtis et al. (2010)
	Organic matter	Schieber (2010), Milner et al. (2010)

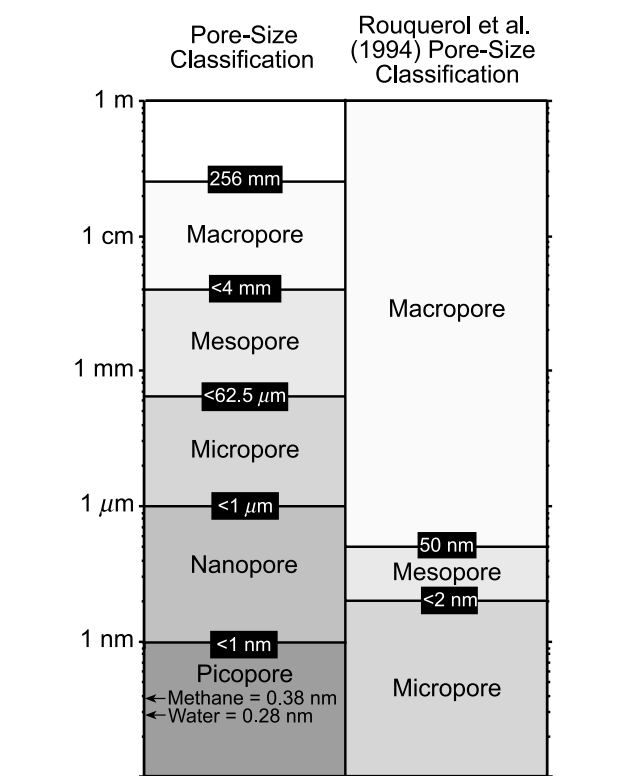


Figure 3. Pore-size classification for mudrock pores. Classification is modified from the Choquette and Pray (1970) classification. New pore classes include a picopore defined as being less than 1 nm and a nanopore defined as being equal to or greater than 1 nm and less than 1 μm . Rouquerol et al. (1994) pore-size classification is also presented because this classification has been suggested as a pore classification for mudrocks. The sizes of methane and water molecules are shown for reference.

increase. At the time of deposition, interP pores occur between grains that range from soft and ductile to hard and rigid. Examples of ductile grains include clay flocculates, peloids (micritic grains of uncertain origin), fecal pellets, and OM; examples of rigid grains include quartz, feldspars, authigenic pyrite, and skeletal material. During burial, ductile grains can distort and close interP pore space and plug pore throats.

In young shallow-buried muds, interP pores have a variety of shapes (Figure 5) (also see Desbois et al., 2009, their figures 3, 4; Milliken and Reed, 2010, their figure 11). In an example of a relatively shallow (1161.5 ft [354 m]) Pliocene–Pleistocene mudrock sample shown in panels A to C of Figure 5, interP pores are elongate and appear not to show a strong preferential orientation. Some of the pores, especially the larger pores, are concentrated around rigid grains (Figure 5A–C). The long dimensions of visible pores range from about 30 nm to 2 μm , which are similar to dimensions of interP mudrock pores shown by Milliken and Reed (2010) from the Pleistocene Nankai accretionary prism. In their photomicrograph (their figure 11), interP pore shapes range from elongated to rounded to angular. Many of the pores appear to be concentrated around rigid grains. Pores range in size from about 100 nm to 3 μm . In contrast, the interP pores of

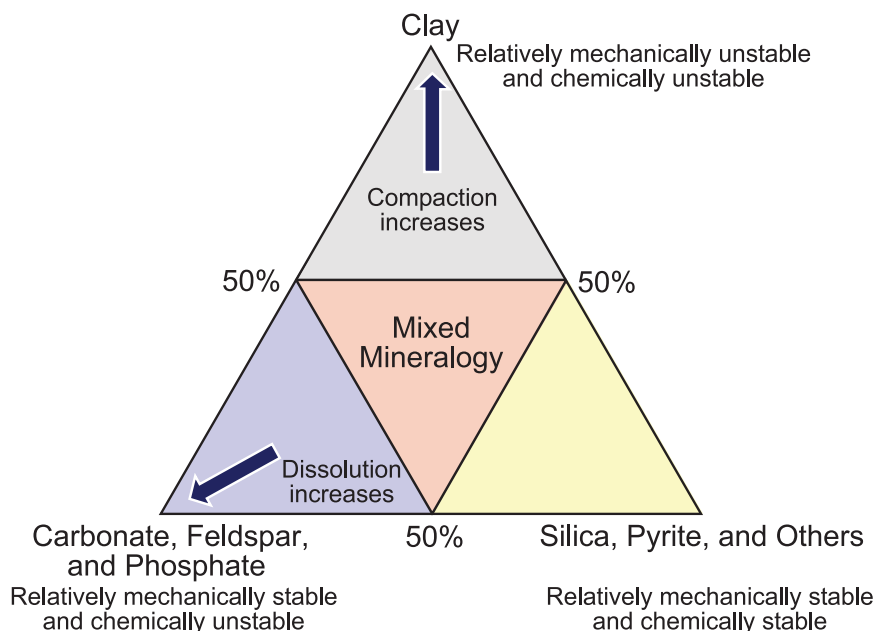


Figure 4. Compositional diagram for mudstones showing stability relationships between mineral end members.

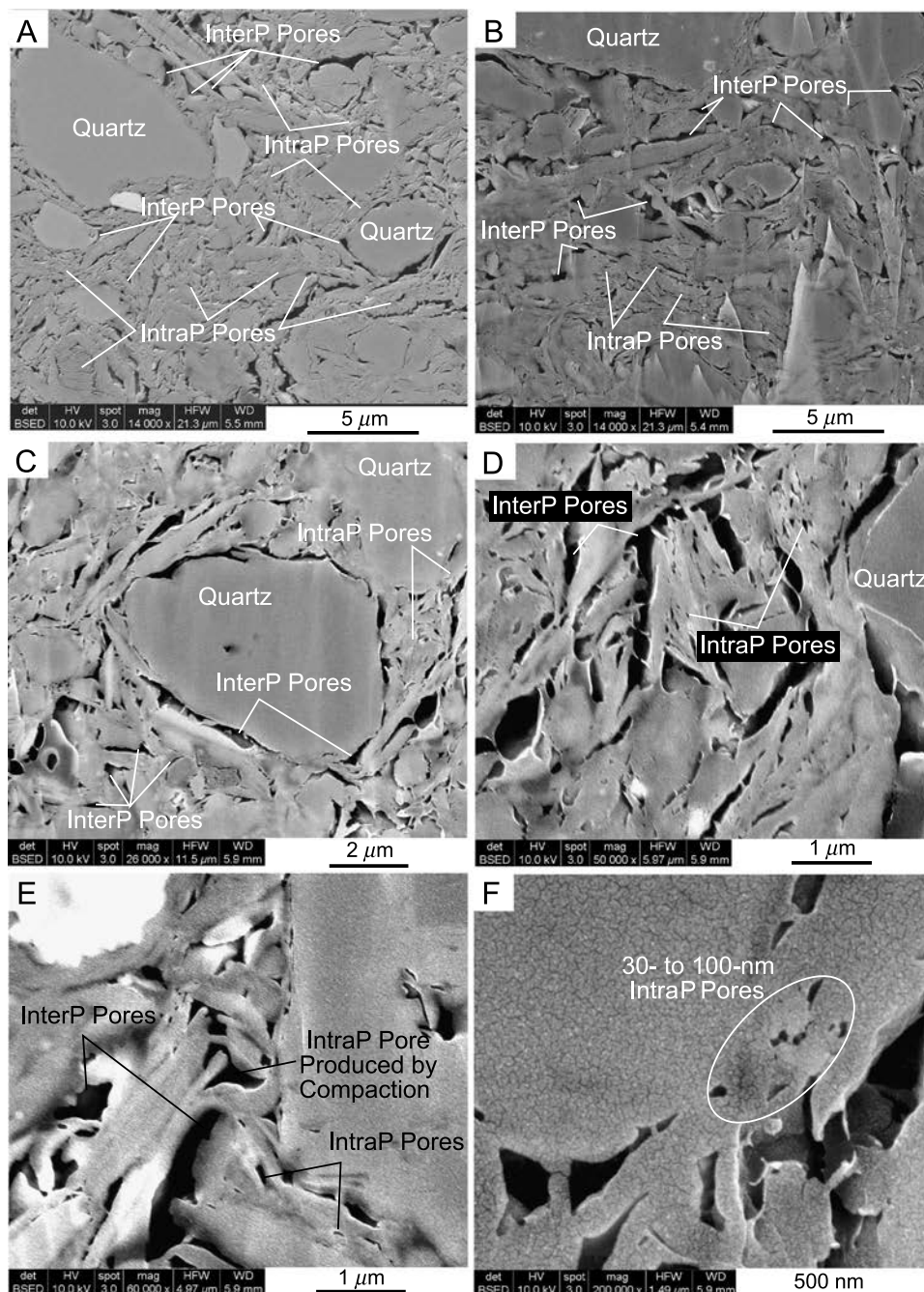
Desbois et al. (2009) from the Oligocene Boom Clay are developed between slightly compacted clay platelets and are elongated roughly parallel to bedding, except where they bend around a rigid grain. Their figure 4D shows a photomicrograph of mud with 20.4% porosity, the pores having lengths of about 35 nm to 2 μm .

In older more deeply buried mudrocks, interP pores are typically reduced in abundance by compaction and cementation (Figures 6, 7). Pores are commonly scattered and show little to no preferential orientation except in localized areas (Figure 6F). Many are triangular and are interpreted to be the remaining pore space between compacted and cemented rigid grains (Figures 6; 7E, F). Others occur as linear pores interpreted to be remnant space between larger clay platelets (Figure 7A). Most pores have lengths in the 1- μm range but can range from 50 nm to several micrometers. Some interP pores may have developed where more ductile grains bend around a rigid grain or preserved where a cluster of rigid grains formed a sheltering effect, inhibiting compaction of the ductile grains (Desbois et al., 2009; Schieber, 2010). The Pliocene–Pleistocene mudstone in Figure 5 displays some excellent examples of this phenomenon. Interparticle pores are not reduced or destroyed only by compaction, but also by cementation around grains such as quartz, calcite, and feldspar (Figure 6A).

Pore-filling cements include authigenic clay minerals (Figure 6B), quartz, and carbonate, as well as less common albite and pyrite. After extensive cementation, identification of individual grain boundaries may be difficult.

We use the term “interparticle” descriptively to categorize pores that occur between particles and crystals. The origin of these pores is varied, and their geometries differ significantly as a function of both primary pore preservation and diagenetic alteration. Accordingly, they commonly require a detailed study of their history so that their origin may be deciphered, and it is best not to use subjective terms requiring this knowledge to categorize them. In Figure 1A, we diagrammatically illustrate some of the most common interP pore types. Pores found between particles are commonly triangular or elongate in cross section (Figure 6A, B). Many of these pores are primary in origin. Grain-edge pores are found along the edge of particles and are possibly related to matrix separating from the particle during compaction. This is also commonly noted adjacent to large OM particles. Interparticle pores are commonly found between clay and mineral particles or between ductile clay and rigid particles (Figures 5A–C, 6F, 8A–D). Intercrystalline pores occur between crystals (Figure 6B). Interparticle pores also occur between clay aggregates that may be compacted clay flocculates (Figure 5).

Figure 5. Example of a relatively shallow-buried (1162 ft [354 m]) Pliocene–Pleistocene clay-rich mudstone from the Ursa Basin (Gulf of Mexico), Integrated Ocean Drilling Program Expedition 308, Site U1324B (Day-Stirrat et al., 2010b). (A) Silty clay-rich mudstone with abundant interparticle (interP) and intraparticle (intraP) pores. Some cleavage intraP pores are enhanced by bending related to compaction. Day-Stirrat et al. (2010b) reported this sample to have 38% porosity. A 2000-point count on this photomicrograph gives values of 13.1% interP pores and 14.5% intraP pores for total visible point-count porosity of 27.6%, far less than the measured porosity. The difference is attributed to pores too small to be counted in the photomicrograph. (B) Similar to A. (C) Interparticle pores are concentrated around the rim of rigid grains. (D) Intraparticle pores are located along cleavage planes of clay particles. (E) Some clay intraP pores are produced during compaction by distortion of clay palettes. (F) Intraparticle pores in the low nanometer size range. det = detector; WD = working distance; mag = magnification; SE2 = secondary electron detector; TLD = through-lens detector; HV = high voltage (accelerating voltage); HFW = horizontal frame width; spot = spot size; BSED = backscattered electron detector.



Intraparticle Pores

Intraparticle pores are found within particles (Figures 1A, 8, 9); most of these are intragranular, but intercrystalline pores are also locally common. Some of these pores are primary in origin, although most are probably diagenetic. Examples include (1) moldic pores formed by partial or complete dissolution, (2) preserved intrafossil pores, (3) intercrystalline pores within pyrite framboids, (4) cleavage-

plane pores within clay and mica-mineral grains, and (5) intragrain pores (i.e., within peloids and fecal pellets).

The relative abundance of intraP pores appears to vary with age. For example, in young muds and mudrocks, they can be very abundant. In older mudrocks, they become more uncommon. Examples of intraP pores in young muds and mudrocks are (1) body-cavity pores in fauna and flora, (2) cleavage-plane pores in clay particles (Figure 5)

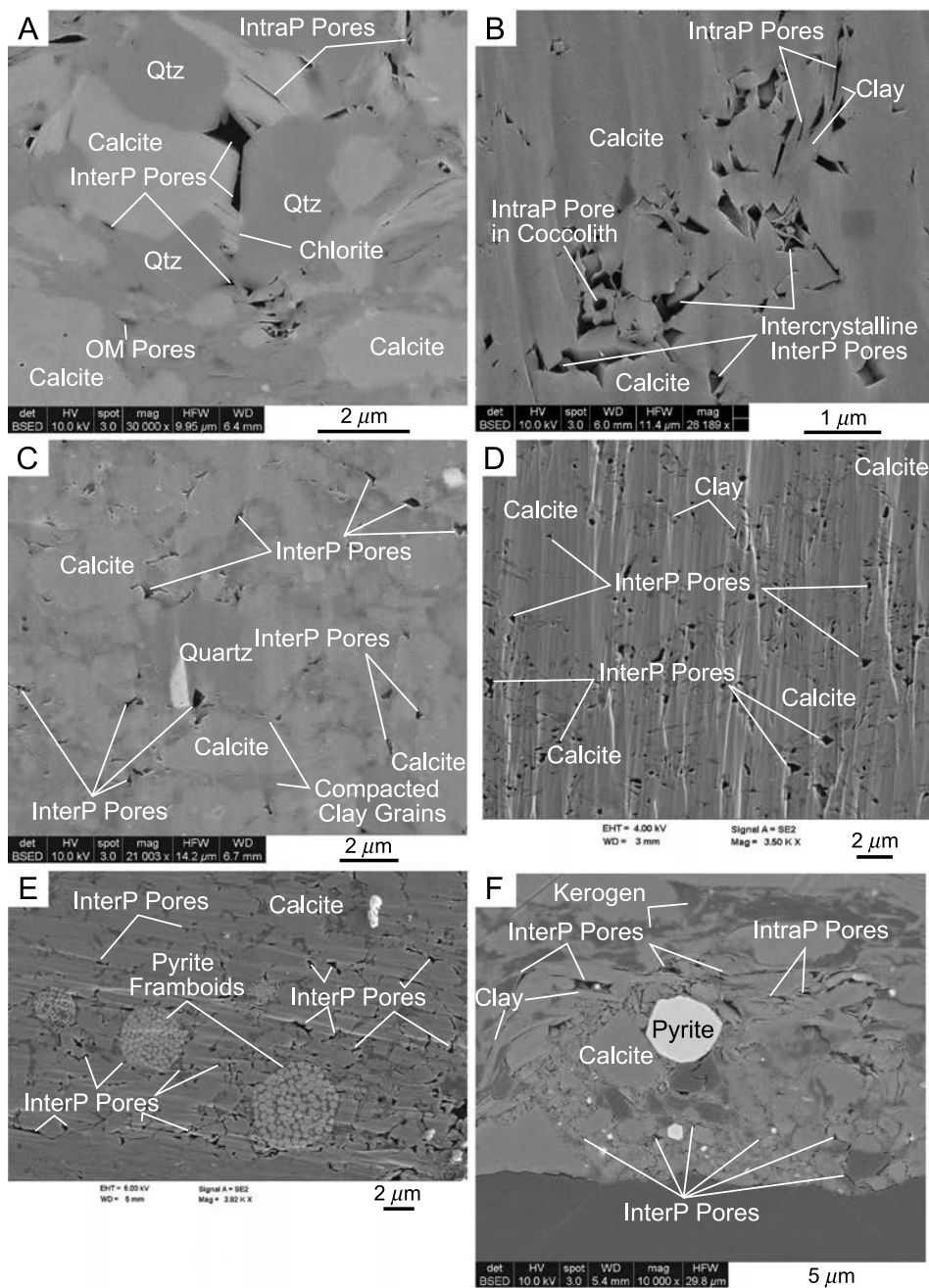


Figure 6. Example of interparticle (interP) pores within mudrocks. (A) Interparticle pores between quartz (Qtz) and calcite grains with cement overgrowths. The interP pores have straight edges, and one pore has a triangular cross section. Intraparticle (intraP) and organic-matter (OM) pores are also present; 8427 ft (2569 m), vitrinite reflectance (R_o) = 1.5%, Lower Cretaceous (lower Bexar Shale Member) Pearsall Formation, Maverick County, Texas. (B) Sample contains intercrystalline-appearing interP pores. Intraparticle pores are also present in the center of the coccolith and along cleavage planes of distorted clay grains; 6900 ft (2103 m), 0.9% R_o , Upper Cretaceous Austin Chalk, La Salle County, Texas. (C) Common interP pores in a mixture of rigid calcite grains and compacted clay grains; 11,734 ft (3577 m), 1.8% R_o , Lower Cretaceous (lower Bexar Shale Member) Pearsall Formation, Maverick County, Texas. (D) Interparticle pore-dominated calcareous mudstone; 13,701 ft (4176 m), 1.5% R_o , Upper Cretaceous Eagle Ford Shale, Dewitt County, Texas. (E) Argillaceous calcareous mudstone has interP pore network, with pores characterized by straight boundaries; 14,381 ft (4383 m), 2.66% R_o , Upper Jurassic Bossier Shale, Sabine County, Texas. (F) Organic-rich argillaceous mudstone with abundant interP pores and some intraP pores. The interP pores have a large range in size (nanometer to micrometer), and some appear to have formed by bending of clay particles. Kerogen is immature and did not form OM pores; 1899 ft (579 m), 0.5% R_o , Devonian New Albany Shale, Hancock County, Kentucky. det = detector; WD = working distance; mag = magnification; SE2 = secondary electron detector; TLD = through-lens detector; HV = high voltage (accelerating voltage); HFW = horizontal frame width; spot = spot size; BSED = backscattered electron detector; EHT = electron high tension (accelerating voltage).

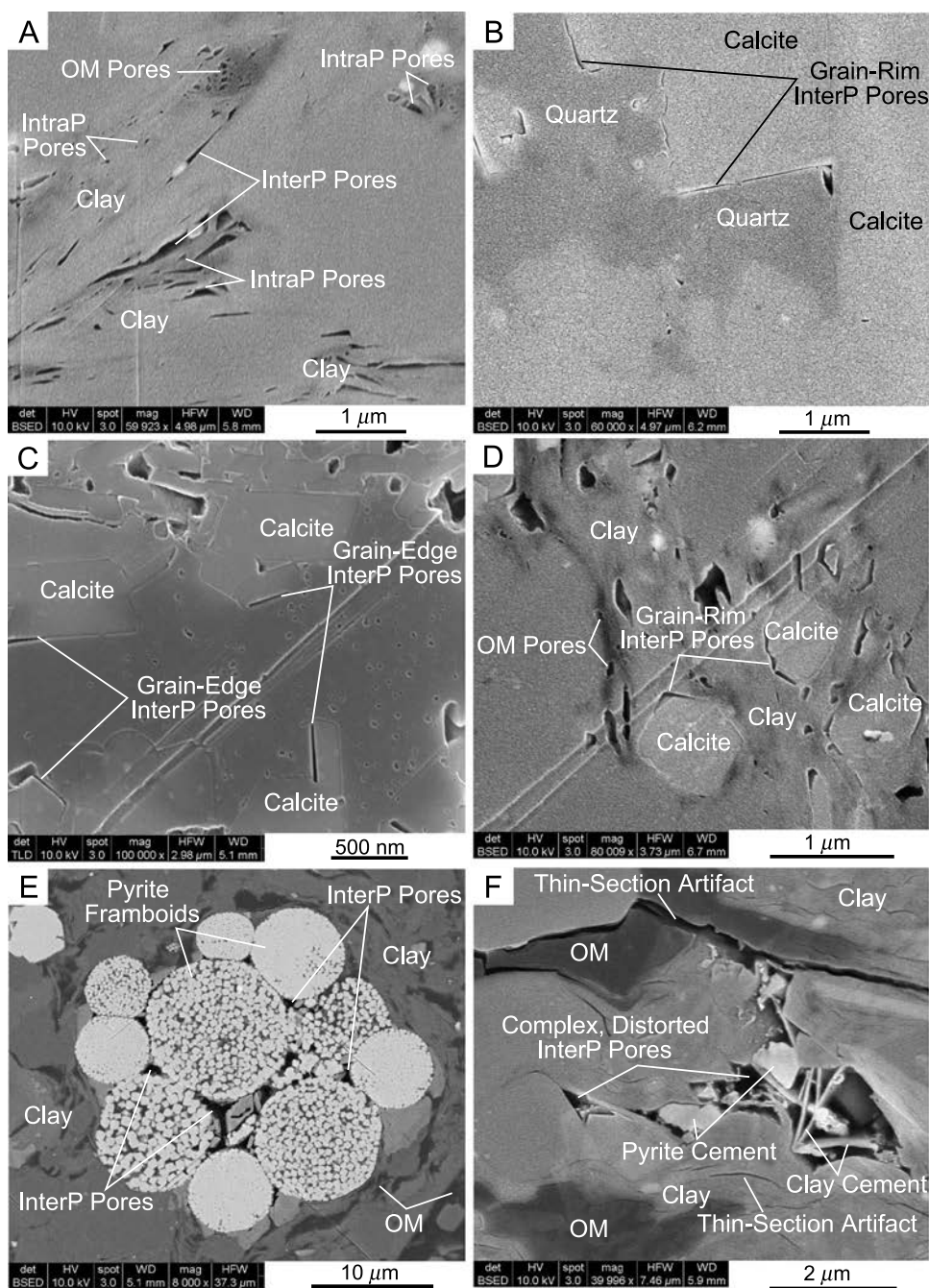


Figure 7. Example of interparticle (interP) pores within mudrocks. (A) Linear interP pore along clay grains. Organic-matter (OM) and intraparticle (intraP) pores present; 10,190 ft (3106 m), vitrinite reflectance (R_o) = 0.85%, Pennsylvanian Atoka interval, Andrews County, Texas. (B) Linear interP pores at contact between quartz crystals and calcite; 10,190 ft (3106 m), 0.85% R_o , Pennsylvanian Atoka interval, Andrews County, Texas. (C) Linear interP pores parallel to edges of calcite crystals; 7103 ft (2165 m), 1.45% R_o , Posidonia Shale (Lower Jurassic), Germany. (D) Grain-edge interP pores along rigid clay-size grains. Organic-matter pores present; 8402 ft (2561 m), 1.5% R_o , Lower Cretaceous (lower Bexar Shale Member) Pearsall Formation, Maverick County, Texas. (E) Interparticle pores between framboids of pyrite; 1879 ft (573 m), 0.5% R_o , Devonian New Albany Shale, Hancock County, Kentucky. (F) Complex interP pore. This relatively large mudstone pore appears to have collapsed after being partly occluded by clay and pyrite cement. Cementation commonly breaks up larger pores into smaller pores; 10,522 ft (3207 m), 1.16% R_o , Pennsylvanian Atoka interval, Midland County, Texas. det = detector; WD = working distance; mag = magnification; SE2 = secondary electron detector; TLD = through-lens detector; HV = high voltage (accelerating voltage); HFW = horizontal frame width; spot = spot size; BSED = backscattered electron detector; TLD = through-lens detector.

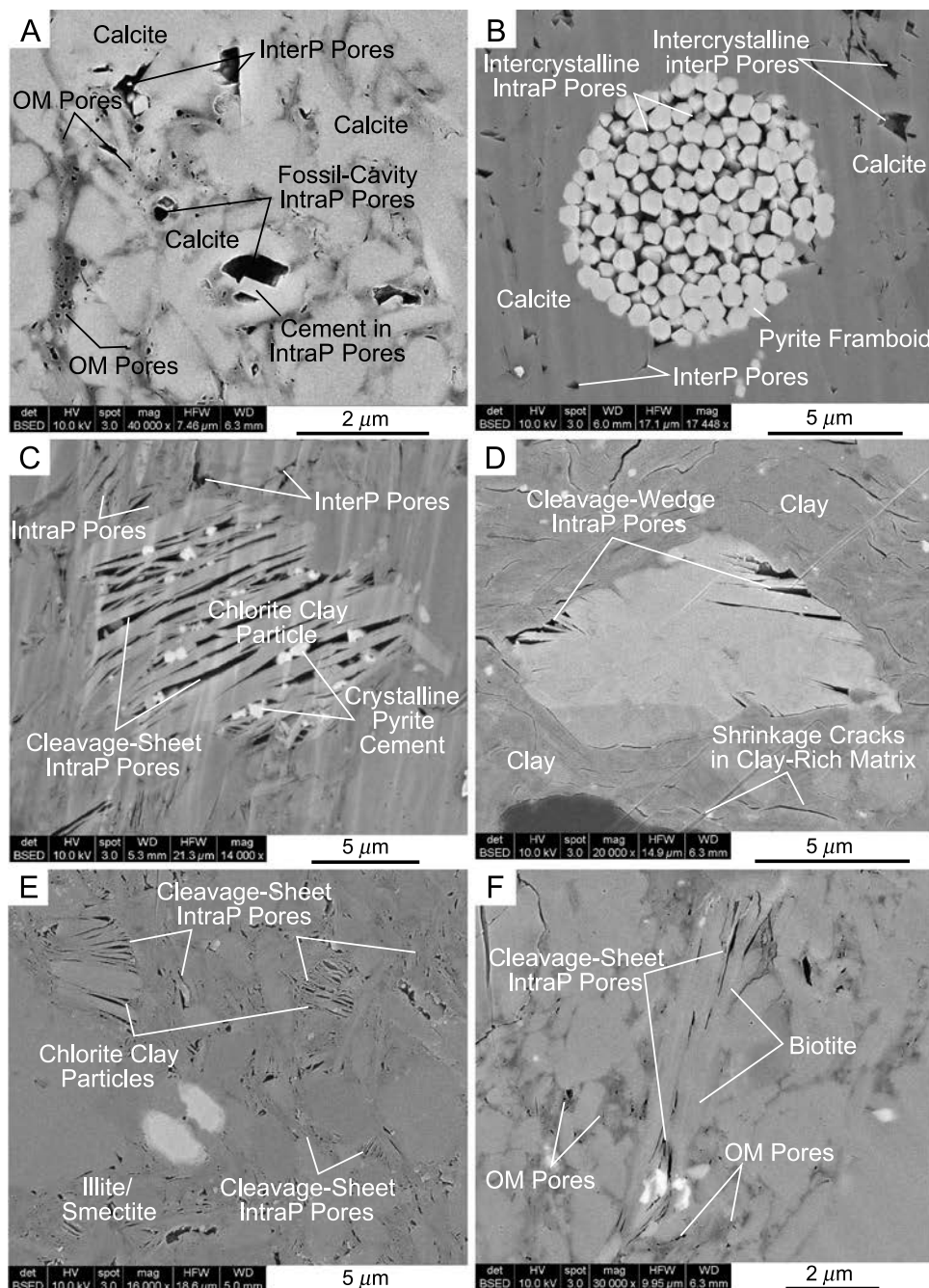
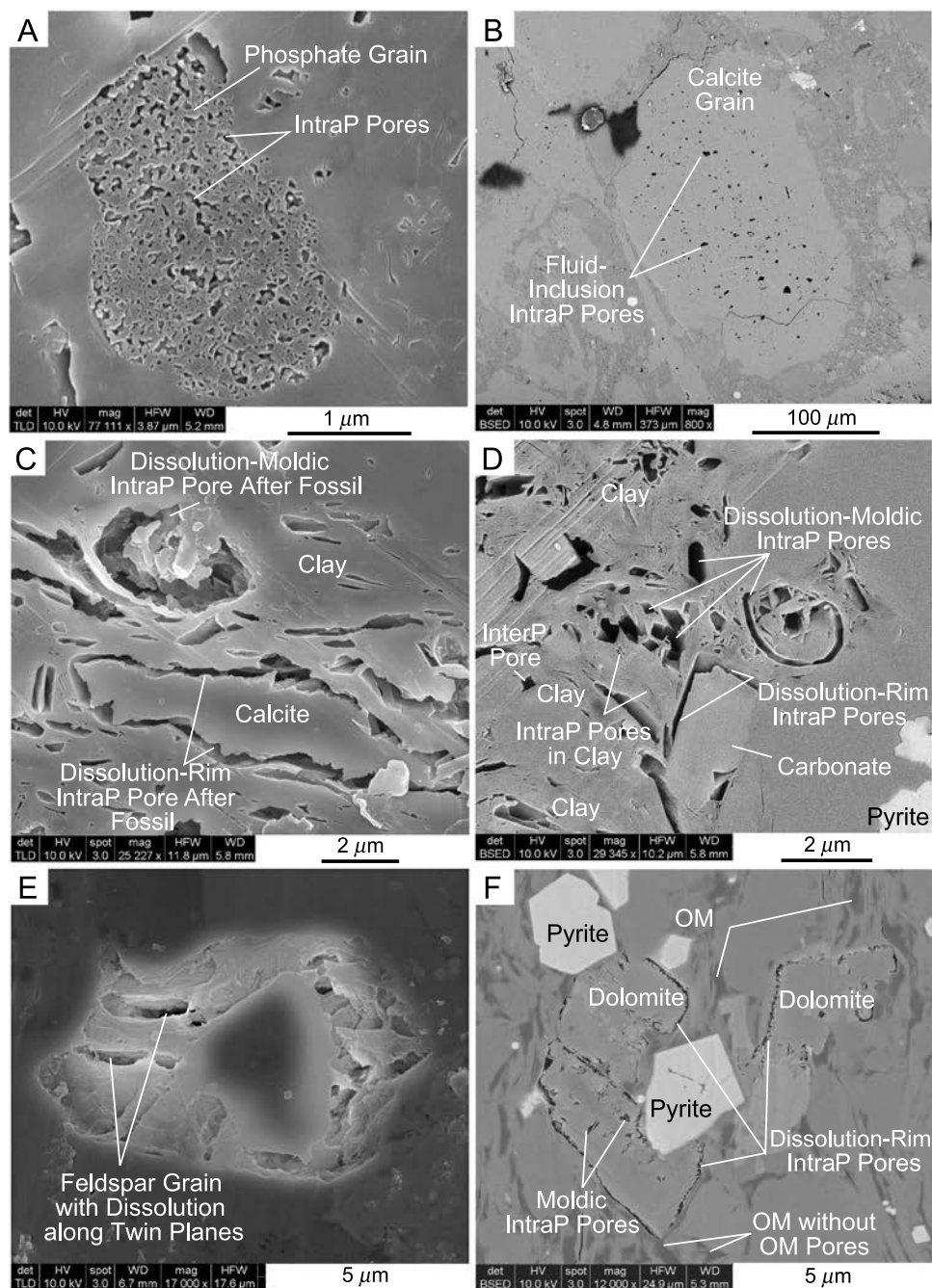


Figure 8. Example of intraparticle (intraP) pores within mudrocks. (A) Sample contains microfossils with interparticle (interP) body-cavity pores. Interparticle and organic-matter (OM) pores are present; 8470 ft (2582 m), vitrinite reflectance (R_o) = 1.5%, Lower Cretaceous (lower Bexar Shale Member) Pearsall Formation, Maverick County, Texas. (B) Intercrystalline intraP pores within a pyrite framboid. Intercrystalline interP pores between calcite crystals have sharp triangular outlines; 6900 ft (2103 m), 0.9% R_o , Upper Cretaceous Austin Chalk, La Salle County, Texas. (C) Cleavage-sheet intraP pores within a clay particle; 11,209 ft (3417 m), 1.3% R_o , Upper Jurassic Haynesville Formation, Harrison County, Texas. (D) Cleavage wedge-shaped intraP pores along boundary of clay particle; 10,460 ft (3188 m), 0.89% R_o , Pennsylvanian Atoka interval, Andrews County, Texas. (E) Sample showing several grains containing cleavage-sheet intraP pores; 13,344 ft (4369 m), 1.24% R_o , Upper Jurassic Bossier Shale, San Augustine County, Texas. (F) Biotite flake containing cleavage-sheet intraP pores. Organic-matter pore present; 8470 ft (2582 m), 1.5% R_o , Lower Cretaceous (lower Bexar Shale Member) Pearsall Formation, Maverick County, Texas. det = detector; WD = working distance; mag = magnification; SE2 = secondary electron detector; TLD = through-lens detector; HV = high voltage (accelerating voltage); HFW = horizontal frame width; spot = spot size; BSED = backscattered electron detector.

Figure 9. Example of intraparticle (intraP) pores within mud-rocks. (A) Intraparticle pores within phosphate grain (pellet?); 8845 ft (2696 m), vitrinite reflectance (R_o) = approximately 1.2%, Lower Cretaceous (lower Bexar Shale Member) Pearsall Formation, Maverick County, Texas. (B) Fluid-inclusion intraP pores within large calcite grain; 13,344 ft (4369 m), 1.24% R_o , Upper Jurassic Bossier Shale, San Augustine County, Texas. (C) Dissolution-rim moldic pores after dissolved fossils; 15,934 ft (4857 m), approximately 1.8% R_o , Lower Cretaceous (Pine Island Shale Member) Pearsall Formation, Bee County, Texas. (D) Dissolution pores after dolomite crystals and fossils. Interparticle (interP) pores present; 15,934 ft (4857 m), approximately 1.8% R_o , Lower Cretaceous (Pine Island Shale Member) Pearsall Formation, Bee County, Texas. (E) Dissolution pores in feldspar-silt grain along twin planes; 2400 ft (732 m), approximately 0.6% R_o , Mississippian Barnett Shale, Wise County, Texas. (F) Dissolution-rim and moldic pores in dolomite crystals; 1879 ft (573 m), 0.5% R_o , Devonian New Albany Shale, Hancock County, Kentucky. OM = organic matter; det = detector; WD = working distance; mag = magnification; SE2 = secondary electron detector; TLD = through-lens detector; HV = high voltage (accelerating voltage); HFW = horizontal frame width; spot = spot size; BSED = backscattered electron detector; TLD = through-lens detector.



and micas, (3) pore spaces within clay flocculates (Figure 5), and (4) pore spaces within fecal pellets.

Desbois et al. (2009) showed excellent examples of intraP pores within clay particles (their figures 3 and 4) of immature mudstones. Because the clay particles in their mudstone example are oriented roughly parallel to bedding, the sheet-

like pores tend to line up parallel to bedding, except where they are bent around a rigid grain (their figure 3A). The shallow-buried Pliocene–Pleistocene claystone presented in Figure 5 shows excellent examples of intraP pores along distorted cleavage planes within clay particles. Some of the intraP pores appear to be within compacted clay

particles that were composed of loosely aggregated clay platelets (Figure 5D). The intraP pores range in size from 10 nm (Figure 5F) to 1 μm (Figure 5A).

In older mudrocks, many of the early formed intraP pores are absent, presumably destroyed by mechanical compaction, or they have been filled in with cement. However, other intraP pores (dissolution intraP pores) develop in the subsurface by corrosive fluids. Milner et al. (2010) and Schieber (2010) also recognized intraP dissolution pores. This dissolution process is addressed in the Discussion section. The shape of an intraP pore is commonly controlled by its origin. In clay particles and micas, pores are sheetlike (Figure 8C–F); in fossils, pores are controlled by the shape of the body cavity (Figure 8A); and in grain and crystal dissolution moldic pores, the pores can take the shape of the precursor (Figure 9C–F). As with other pore types, intraP pores can contain cement (Figure 8A, C) that occludes pore space.

Common types of intraP pores are shown in Figure 1A. Pyrite intercrystalline pores between pyrite crystals are locally common in pyrite framboids (Figure 8B). Many of these pores are occluded with OM or with authigenic clay platelets. Intraparticle pores within clay sheets that may be flocculates are generally linear and are parallel to one another (Figure 8C–E). Similar pores are seen in micas (Figure 8F). Intraparticle pores along crystal rims or grains are most likely formed by partial dissolution of carbonate crystals and grains (Figure 9F). Crystal-mold pores are related pores created by the complete dissolution of a crystal (Figure 9D). Dissolution pores also occur in feldspar grains (Figure 9E). Body-cavity pores include primary pore chambers within faunal and floral fossil grains (Figures 6A, 8A). Fossil molds are the product of diagenetic dissolution of fossil skeletons (Figure 9C, D). Figure 9A shows pores within a possible fecal pellet that are similar to pores described by Milner et al. (2010). Figure 9B shows fluid-inclusion pores within a crystal.

Organic-Matter Intraparticle Pores

Organic-matter pores (Figures 1A, 10, 11) are intraP pores that are found within OM. We have observed

that thermal maturation has to reach an R_o level of approximately 0.6% or higher before OM pores begin to develop, which, according to Dow (1977), is the beginning of peak oil generation. At levels of maturity less than 0.6% R_o , OM pores are absent or extremely rare (Figure 11C). Reed and Loucks (2007), Ruppel and Loucks (2008), and Loucks et al. (2009) were the first to describe the OM pores and associated pore network in the Barnett mudstone play in the Fort Worth Basin. Since then, other studies have also documented the abundance of this pore type in Barnett mudstones (i.e., Sondergeld et al., 2010). Ambrose et al. (2010) and Sondergeld et al. (2010) used SEM–focused ion beam (FIB) analysis to demonstrate that these OM pores formed a connected 3-D effective pore network through the touching of grains, a relationship previously suggested by Loucks et al. (2009). The abundance of this pore type is now well established in most other mudrock systems by the present authors and other researchers (Table 1), including the Eagle Ford, Pearsall, Kimmeridge, Floyd, Woodford, Marcellus, Horn River, and Maquoketa systems.

Organic-matter pores have irregular, bubble-like, elliptical cross sections and generally range between 5 and 750 nm in length. They commonly appear isolated in two dimensions; but in three dimensions, they display connectivity (Figure 10B, C), which has now been illustrated using SEM-FIB analysis (Ambrose et al., 2010; Sondergeld et al., 2010). The amount of porosity within an OM particle in a single sample ranges from 0 to 40% (Loucks et al., 2009; this study). The large piece of OM in Figure 10A has 41% porosity (by point-count method). A broad range can even occur within a single OM grain (Figure 11D). Curtis et al. (2010) identified organic particles having as much as 50% porosity. Some OM has an inherited structure that controls the development and distribution of the pores within a grain (Figure 11A, B).

Not all OM types appear to be prone to the development of OM pores. Limited data collected during this study suggest that type II kerogen may be more prone to the development of OM pores than type III kerogen. The organic particle in Figure 11E, on the basis of appearance and Rock-Eval data, is interpreted as type III kerogen from

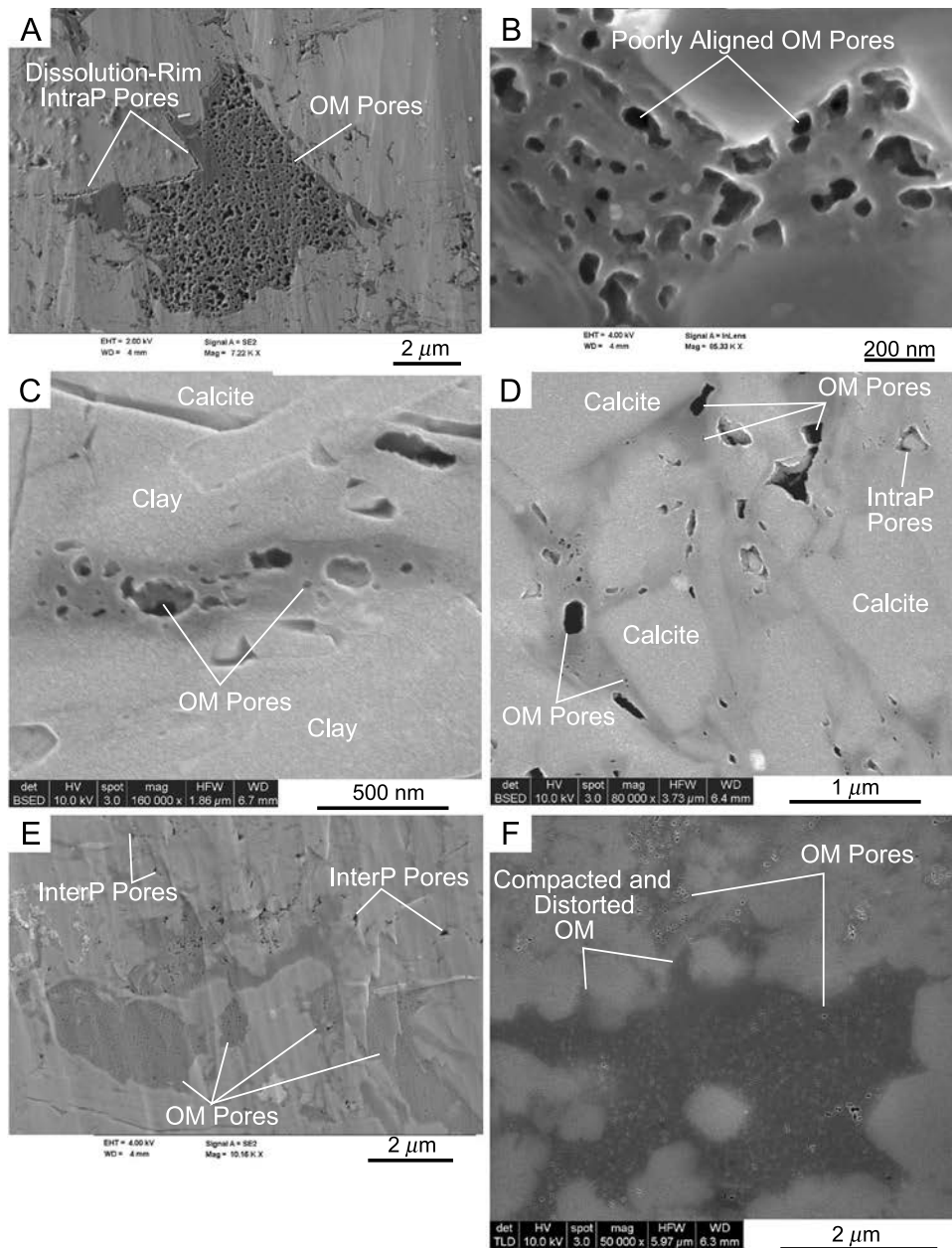


Figure 10. Example of organic-matter (OM) pores within mudrocks. (A) Large OM particle with OM pores. On the basis of point counting 1000 points, this grain has a porosity value of 41%; 7625 ft (2324 m), vitrinite reflectance (R_o) = approximately 1.6%, Mississippian Barnett Shale, Wise County, Texas. (B) Organic-matter pores slightly aligned and showing complexity in third dimension; 7625 ft (2324 m), approximately 1.6% R_o , Mississippian Barnett Shale, Wise County, Texas. (C) Organic-matter pores showing range in pore size from 10 to 300 nm; 8402 ft (2561 m), 1.5% R_o , Lower Cretaceous (lower Bexar Shale Member) Pearsall Formation, Maverick County, Texas. (D) Compacted OM with a range of pore sizes; 8470 ft (2582 m), 1.5% R_o , Lower Cretaceous (lower Bexar Shale Member) Pearsall Formation, Maverick County, Texas. (E) Scattered OM containing numerous OM pores; 7138 ft (2176 m), approximately 1.35% R_o , Mississippian Barnett Shale, Wise County, Texas. (F) Large organic flake with numerous pores. Original ductile particle shows flowage between rigid grains; 12,923 ft (3939 m), 1.31% R_o , Mississippian Barnett Shale, Pecos County, Texas. InterP = interparticle; intraP = intraparticle; det = detector; WD = working distance; mag = magnification; SE2 = secondary electron detector; TLD = through-lens detector; HV = high voltage (accelerating voltage); HFW = horizontal frame width; spot = spot size; BSED = backscattered electron detector.

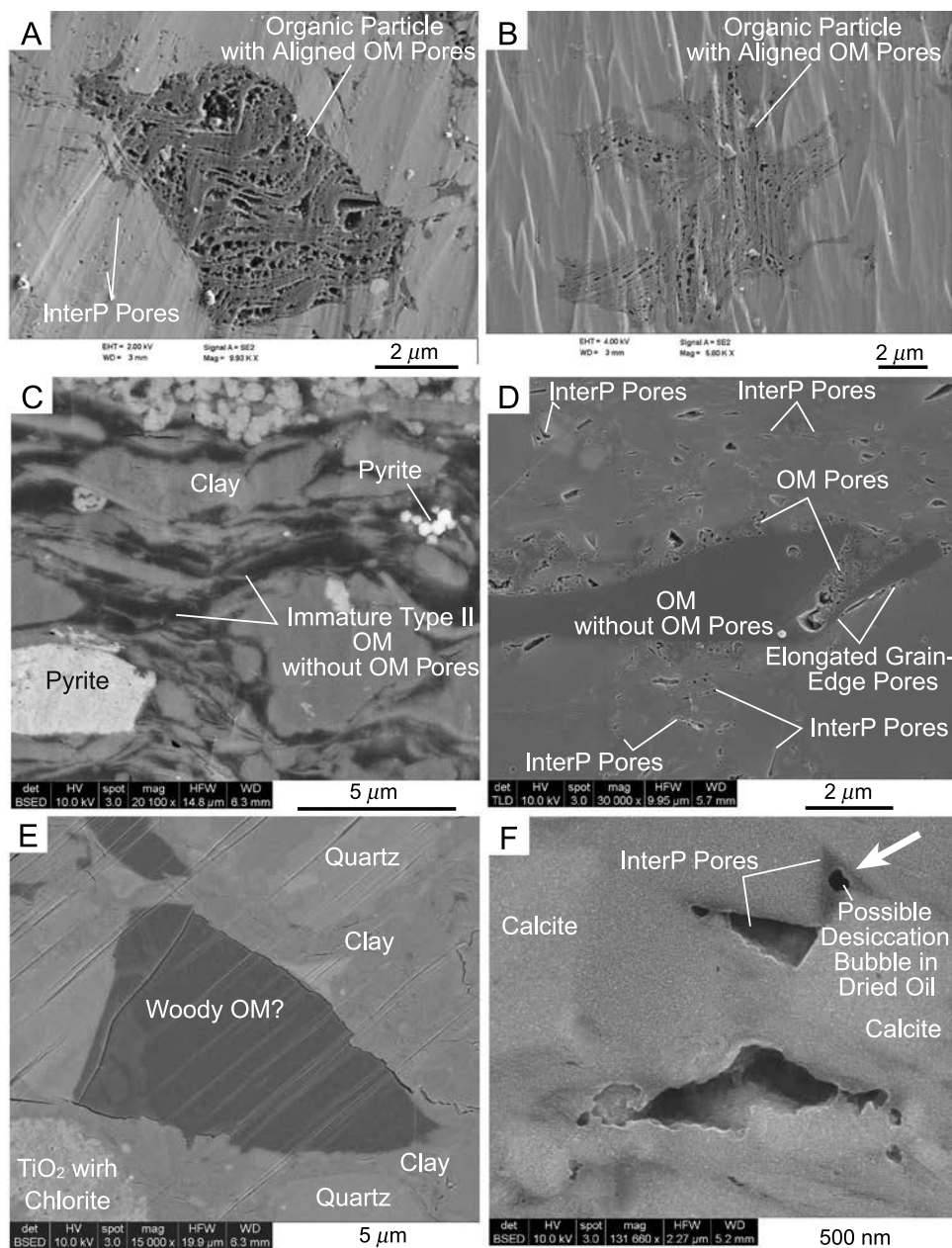


Figure 11. Example of organic-matter (OM) pores within mudrocks. (A) Organic particle with relatively large OM pores showing alignment. The original particle had inherent variation in its internal structure; 7625 ft (2324 m), vitrinite reflectance (R_o) = approximately 1.6%, Mississippian Barnett Shale, Wise County, Texas. (B) Organic-matter pores showing alignment controlled by original structure of OM; 8545 ft (2605 m), 3.17% R_o , Mississippian Barnett Shale, Hill County, Texas. (C) Immature OM in shallow-buried Barnett Shale showing no onset of OM pore development; 647 ft (197 m), less than 0.5% R_o , Mississippian Barnett Shale, Lampasas County, Texas. (D) A large piece of kerogen showing areas of OM pore development and other areas free of OM pores. This examples shows elongate grain-edge pores that may be associated with separation of the grain from the matrix during compaction; 15,934 ft (4857 m), approximately 1.8% R_o , Lower Cretaceous (Pine Island Shale Member) Pearsall Formation, Bee County, Texas. (E) Woody-type kerogen showing no development of OM pores. This type of kerogen may not be prone to OM pore development; 10,460 ft (3188 m), 0.89% R_o , Pennsylvanian Atoka interval, Andrews County, Texas. (F) Interparticle (interP) pore (arrow) may have been originally filled with oil. A possible shrinkage bubble formed in the center of the pore after drying. Pores associated with residue oil and could be mistaken for kerogen-type OM pores; 9700 ft (2957 m), 0.78% R_o , Lower Cretaceous (Pine Island Shale Member) Pearsall Formation, Atascosa County, Texas. det = detector; WD = working distance; mag = magnification; SE2 = secondary electron detector; TLD = through-lens detector; HV = high voltage (accelerating voltage); HFW = horizontal frame width; spot = spot size; BSED = backscattered electron detector; EHT = electron high tension (accelerating voltage); TLD = through-lens detector.

the Atoka in the Midland Basin, and it shows no development of OM pores, despite having an R_o of 0.89%. No OM pores were observed in this unit. Schieber (2010) also noted that the type of OM may control OM pore formation in thermally mature rocks.

Note that imaging pores with residual oil can lead to the mistaken identification of OM pores. Figure 11F shows what we think may be residual oil within an interP pore. The darker material in the pore is some form of organic material. Because the bubble-shaped pore is in the center, it appears to be a desiccation pore resulting from oil in the pore drying out and, therefore, not an OM pore.

Comparisons with Previous Pore Naming and Classification Schemes

Previous authors have used a variety of both descriptive and interpretive names to characterize mudrock pores. Essentially all of these pore types can readily fit into our mudrock pore classification scheme (Tables 1, 2). Many of the names given these pores by previous authors are descriptive and, thus, useful for describing specific pore subtypes within the threefold system we propose here. However, we think that interpretive names (e.g., organophyllic, organophobic, carbonate dissolution pores, primary, secondary), although useful when supported by pore genesis data, should be avoided in any pore classification scheme.

Fracture-Related Pores

Fracture-related pores are not part of the matrix-related pore classification presented in this article; however, these nonmatrix pores can be very important in shale-gas systems where they exist and are not completely cemented. Where natural fractures are present in mudrock reservoirs, they can have a significant effect on hydrocarbon production (Eichhubl and Boles, 1998; Pitman et al., 2001; Clarke, 2007; Gale and Holder, 2010). Some mudrock reservoirs have fractures that are cemented and impermeable. Nevertheless, they can still have a strong influence on induced fracture propagation (Gale et al., 2007). Pearsall mudstones have opening-

mode natural fractures that contain pores between calcite cement fill (Figure 12A). Early successful wells in the Pearsall mudstones have been attributed to open fractures (Clarke, 2007). Open microfractures have also been thought to be present in mudrocks (Kanitpanyacharoen et al., 2011, their figures 4, 5) and as a storage and transport mechanism for hydrocarbons in mudrocks (e.g., Dewhurst et al., 1999). However, no quantity of open microfractures has been found in the hundreds of samples that we have investigated using thin-section and SEM-based imaging. One cemented microfracture has been noted in the Barnett Shale (Loucks et al., 2009), and one partly cemented microfracture was identified in an Atokan mudstone (Figure 12B). Although large, permeable, natural fractures may be present in some mudrocks, abundant open microfractures have yet to be well documented at the thin-section or SEM scale by this study of hundreds of samples.

MUDROCK PORE NETWORKS AND ASSOCIATED PORE ABUNDANCE AND DISTRIBUTION

Mudrocks may contain one dominant pore type or a combination of pore types. Understanding the abundance, distribution, and spatial interrelationships of each pore type is important because each type may contribute differently to permeability, leading to the need to understand the distribution of pores and establish their connectivity. Mudrock reservoirs have inherently low permeability and require fracture stimulation to improve hydrocarbon flow. We must, therefore, recognize the permeability pathways within the mudrock matrix to induced fractures.

To address the questions of pore distribution and connectivity, we point counted pores of ion-milled samples from four typical mudrocks using photomicrographs taken on the SEM. Three samples come from major producing mudstone reservoir systems (Barnett, Pearsall, and Bossier); one comes from a shallow, young, nonproductive, Pliocene–Pleistocene claystone (Figures 5A, 13). Proportions

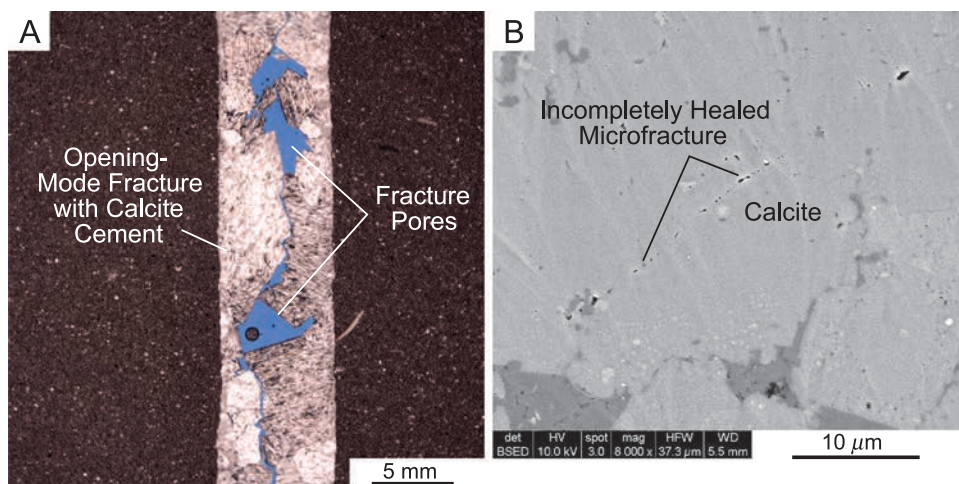


Figure 12. Examples of fracture pores. (A) Opening-mode fracture partly filled with calcite cement. Some fracture pores open; 8524 ft (2598 m), Lower Cretaceous (lower Bexar Shale Member) Pearsall Formation, Maverick County, Texas. (B) Example of a rare natural microfracture, approximately 30 μm long, 0.1 μm wide, and partly healed; 10,140 ft (3091 m), Pennsylvanian Atoka interval, Andrews County, Texas.

of pore types are plotted on the ternary diagram in Figure 1B.

The Pliocene–Pleistocene sample (Figure 5A) is a silty claystone with an estimated R_o of less than 0.3%. Visible porosity, on the basis of 1000 point counts, is 27.6%. Pores are nearly equally divided between interP (47.5%) and intraP (52.5%). According to Day-Stirrat et al. (2010b), this sample has a measured porosity of 38% (measured by mercury injection capillary pressure analysis), which is higher than the visible point-count porosity. The difference between these two measurements is likely the result of pores being too small to be point counted on the photomicrograph.

The Barnett sample (Figure 13A) is a calcareous siliceous mudstone with abundant OM (original total organic content by point count [volume percent] was $\sim 12.4\%$) and about 1.35% R_o . Visible porosity, on the basis of 2000 point counts, is 4.2%. Pores are dominantly within OM (95.2%), with some intraP pores (4.8%). Trace amounts of interP pores are also present. Most of the OM contains well-developed pores, and it displays extensive compaction and deformation around rigid grains.

Although similar in maturity ($\sim 1.24\%$ R_o), the Bossier sample, an argillaceous calcareous mudstone (Figure 13B), differs significantly in visible porosity and pore abundance from the Barnett sample. Porosity, on the basis of 2000 point counts, is 7.2%. Intraparticle pores are most abundant (75.5%), followed by interP (19.6%) and OM pores (4.9%). Most of the intraP pores are associated with dis-

torted cleavage planes in micas and clay-rich grains. Some of the interP pores are grain-edge pores.

The Pearsall sample (Figure 13C) is a siliceous, calcareous mudstone with 1.5% R_o . Porosity, on the basis of 2000 point counts, is only 1.8%. Most pores are interP (69.4%), with the rest being mostly intraP (30.6%). Organic-matter pores are uncommon. Some of the interP pores are grain-edge pores. Intraparticle pores occur within micas or as fluid inclusions in calcite grains.

These four mudstone examples illustrate the broad variety of pore networks that can exist in mudrocks, depending on age, mineralogy, and OM type and content. Plotting them on the ternary pore classification (Figure 1) provides a quick comparison of the pore networks.

DISCUSSION

Pore Types and Effective Pore Networks

That the permeability of carbonate and coarse-grained siliciclastic pore networks are related to pore types is well known (i.e., Pittman, 1979; Lucia, 1999). Interparticle pores are generally better connected to one another than intraP pores. Therefore, higher permeability is generally related to interP pore networks than to intraP pore networks. Intraparticle pores are commonly connected to the overall pore system, but associated pore throats may be smaller and relatively fewer than those associated with

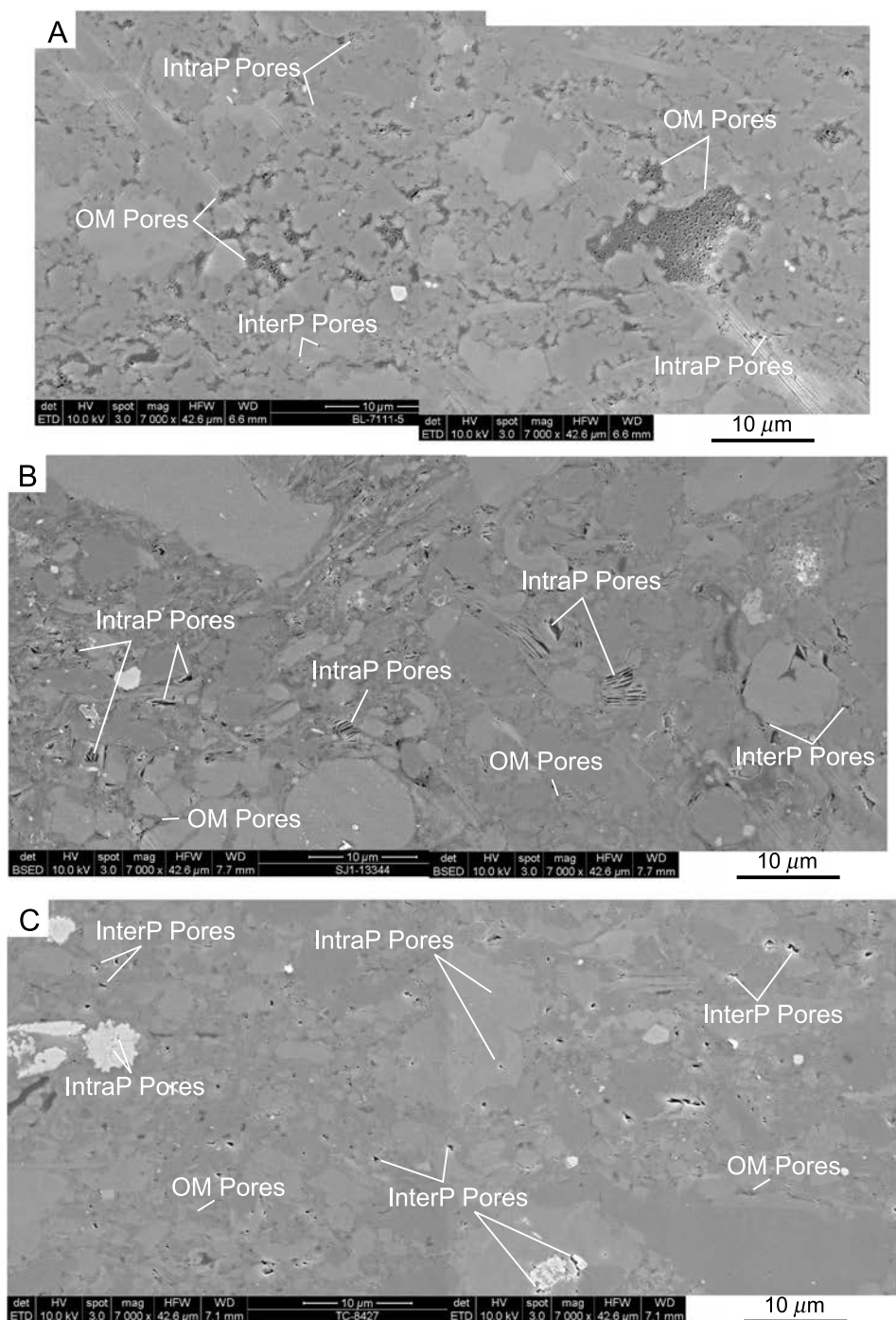


Figure 13. Examples of mudrock-pore networks. Percent matrix, total organic content (TOC), organic-matter (OM) pores, interparticle (interP) pores, and intraparticle (intraP) pores calculated by point counting 2000 points. (A) Organic-rich calcareous siliceous mudstone with OM pore-dominated pore network. Present TOC = 8.4% and original TOC = 12.4%. Total point-count porosity = 4.2%, of which OM pores = 95.2%, interP pores = 0%, and intraP pores = 4.8% of pore volume; 7111 ft (2167 m), vitrinite reflectance (R_o) = approximately 1.35%, Mississippian Barnett Shale, Wise County, Texas. (B) Siliceous calcareous mudstone with intraP pore-dominated pore network. Present TOC = 0.9% and original TOC = 1.3%. Total point-count porosity = 7.2%, of which OM pores = 4.9%, interP pores = 19.6%, and intraP pores = 75.5% of pore volume; 13,344 ft (4067 m), 1.24% R_o , Upper Jurassic Bossier Shale, San Augustine County, Texas. (C) Siliceous calcareous mudstone with interP pore-dominated pore network. Present TOC = 0.3%. Total point-count porosity = 1.8%, of which OM pores = 0%, interP pores = 69.4%, and intraP pores = 30.6% of pore volume; 8427 ft (2569 m), approximately 1.5% R_o , Lower Cretaceous lower Bexar Shale Member of the Pearsall Formation, Maverick County, Texas. det = detector; WD = working distance; mag = magnification; SE2 = secondary electron detector; TLD = through-lens detector; HV = high voltage (accelerating voltage); HFW = horizontal frame width; spot = spot size; BSED = backscattered electron detector; ETD = Everhart-Thomley detector.

interP pores (McCreesh et al., 1991). Some intraP pores, such as moldic pores, may be nearly totally cut off from the effective pore network. We suggest that the same principles of pore connectivity apply to pores in mudrocks. Interparticle pores contribute more to the effective pore network than do intraP pores.

The relative connectivity of OM pores, a form of intraP pores, do not parallel intraP pores in the mineral matrix. As previously noted, several studies have shown that OM pores in a continuous organic framework can form an effective pore system and can form the dominant flow pathway (Loucks et al., 2009; Ambrose et al., 2010; Curtis et al., 2010).

Effect of Mineralogy and Fabric on Pore Development and Preservation

Figure 4 summarizes the importance of mineralogical composition on the development and preservation of mudrock pores. This ternary diagram groups major mudrock minerals by mechanical and chemical stability. The apices are (1) phyllosilicate clay, (2) silica + pyrite, and (3) carbonate + feldspar + phosphate. Each apex reflects different mechanical and chemical stability parameters during diagenesis. Clays are ductile and compact and deform easily, making them mechanically unstable. Many types of clay, especially smectite, are chemically unstable and will transform to mixed-layer clays and illite with increasing temperature associated with burial (i.e., Pytte and Reynolds, 1988). Silica + pyrite are rigid grains that resist compaction and act as focal points where more ductile grains, such as clay and OM, compact around them. They are also relatively chemically stable and generally do not undergo dissolution. Carbonate + feldspar + phosphate are rigid grains and resist compaction. They can also form focal points where more ductile grains will bend and deform. However, they can be chemically unstable and undergo dissolution, forming intraP moldic pores.

The above three end members are important controls on mudrock pore types, but the addition of reactive kerogen is an additional parameter that can greatly affect the pore network system. Given abundant kerogen, a continuous pore network may

develop, such as seen in the Barnett shale-gas system (Loucks et al., 2009; Curtis et al., 2010).

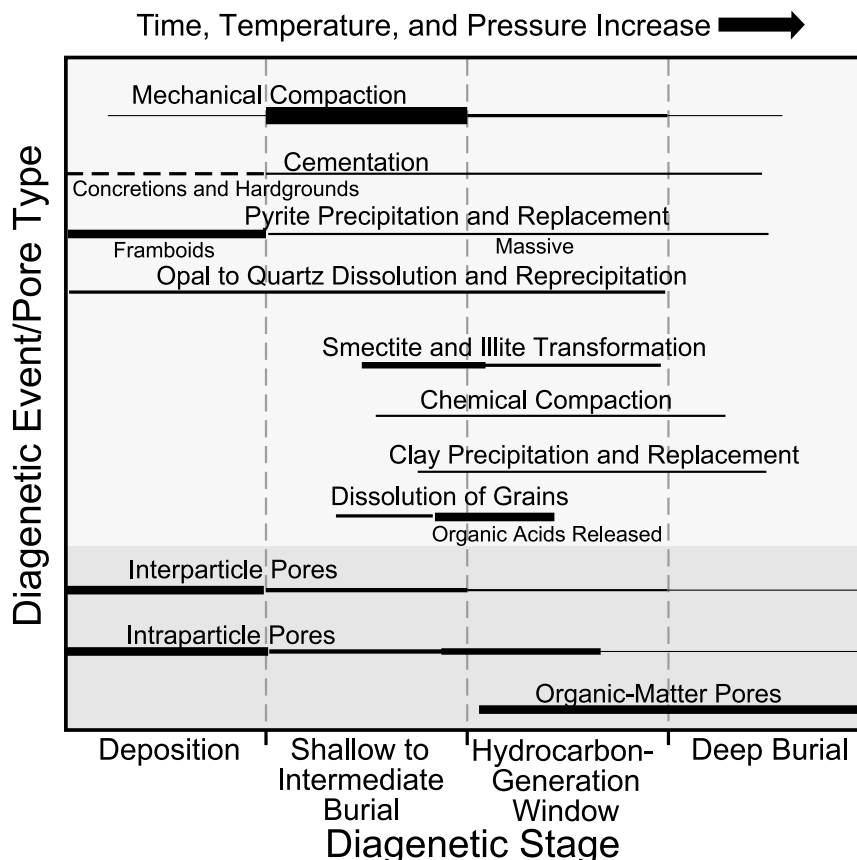
Several authors have noted that admixtures of rigid and ductile grains can affect pore development and preservation (Dawson and Almon, 2002; Desbois et al., 2009; Schieber, 2010; this study). Desbois et al. (2009) described how clay sheets folded around rigid grains can form crescent-shaped pores. Schieber (2010) recognized that pores can be preserved in the compaction-protected shadow adjacent to rigid grains. The Pliocene–Pleistocene sample shown in Figure 5 demonstrates the interaction between ductile and rigid grains. Micrometer-size interP pores developed around the larger rigid grains where ductile clay grains were distorted. Similar pore types are seen in older, more deeply buried mudrocks (Figure 6F). Also observed in this sample are the bending of clay grains and the associated development of intraP sheetlike pores.

Evolution of Mudrock Pores through Time and with Burial

It has been well established that as muds are buried and exposed over time to higher temperatures and pressures, they decrease in volume and become lithified. Initial porosities of muds range from 60 to 80% at the time of deposition (Bridge and Demicco, 2008), and these porosities drop to as low as a few percent in the subsurface. As an example of porosities in producing shale-gas reservoirs, TXCO (2009) noted porosity ranges in several shale-gas systems: (1) Barnett Shale from 4.0 to 9.6%, (2) Haynesville Formation from 8 to 15%, (3) Fayetteville Shale from 4.0 to 5.0%, (4) Pearsall Formation from 6.0 to 11.5%, and (5) Eagle Ford from 3.4 to 14.6%. No information was provided on how the porosity ranges were calculated. The burial diagenesis and transformation of muds to mudrocks is a complex process composed of many variables and controls, including original mineralogy, fabric, texture, organic content, fluids, hydrology, and rate and depth of burial. Figure 14 illustrates some of the major processes involved in the evolution of mud to mudrocks.

Perhaps the most significant process in mud diagenesis is mechanical compaction. Bridge and

Figure 14. Generalized parasequence summary diagram of the major stages in mudrock burial diagenesis and the relationship of these stages to the evolution of pore types and abundances in mudrocks. This sequence of diagenetic events does not reflect any particular case history of a specific mudrock.



Demicco (2008) noted that the fastest rates of compaction occur in the first kilometer (0.6 mi) of burial, which is before major mineralogical diagenesis starts, except for limited carbonate, phosphate, and early pyrite diagenesis. This rapid rate of compaction has been documented by many studies (i.e., Rieke and Chilingarian, 1974; Fruehn et al., 1997; Van Sickel et al., 2004). Most compaction occurs before the initiation of any significant volume of hydrocarbon generation. Bridge and Demicco (2008) also noted that major large-scale mineral transformations do not begin until temperatures of approximately 100°C are reached. Therefore, during much of the early history of burial, interP and intraP pores are primarily lost through compaction. During this time, ductile grains are distorted and flow into interP pores between rigid grains, adding to the loss of interP pore space.

Some early cementation can occur in near-surface settings in the form of carbonate (i.e., Raiswell, 1976), pyrite (i.e., Wilkin et al., 1996,

1997), and phosphate (i.e., Föllmi, 1996) minerals. These diagenetic products commonly form as concretions and hardgrounds (i.e., Weeks, 1957) and effect minimum volumes of sediment. Loucks and Ruppel (2007) recognized each of these early diagenetic products in the Barnett Shale. Siliceous ooze (i.e., diatoms, radiolarians, silicoflagellates, and sponges) with an opal mineralogy will undergo a transformation through opal A, to opal CT, to cryptocrystalline quartz (i.e., Kastner et al., 1977; Williams and Crerar, 1985). This solution-redeposition mechanism may simply transform the siliceous particles in place or reprecipitate-dissolved silica in pores. Work by Matheney and Knauth (1993), based on isotope evidence from the Miocene Monterey Formation, stated that it is a relatively low-temperature process starting at 17 to 21°C.

The process of diagenetic transformation of smectite to illite during burial is well known (i.e., Boles and Franks, 1979). During this process, elements can be released, and volume changes occur

(Day-Stirrat et al., 2010a, c). Silica, calcium, and others can be released from the clays, forming new authigenic clays and minerals (Hayes, 1991; Surdam et al., 1991; Land and Milliken, 2000; Day-Stirrat et al., 2010c; Schieber, 2010) that occlude pore space. Figure 14 suggests the relative timing of this transformation event.

Dissolution of carbonates (both aragonite and calcite) and feldspars are noted in mudrocks. Aragonite is unstable with burial and dissolves. Schieber (2010) suggested that fluids for the dissolution process in mudrocks are the fluids associated with decarboxylation of kerogen, which produces an increase of carboxylic and phenolic acids. He suggested that this occurred in the temperature range of 80 to 120°C, following the concept developed by MacGowan and Surdam (1990). These late aggressive fluids could dissolve calcite and feldspar. The dissolved material is reprecipitated in the mudrock unless it migrates out of the system.

General pore evolution history in mudrocks, related to burial diagenesis, is summarized in Figure 14. Given our review of relatively young mudrocks (i.e., Figure 5), pores at and in the shallow subsurface are interP and intraP. During initial burial to several kilometers, interP and intraP are compacted and affected by chemical diagenesis, and the volume of interP and intraP pores greatly decreases. Porosity versus depth curves (Fruehn et al., 1997; Van Sickle et al., 2004) for mud-dominated strata show that porosity can drop to less than 10% by 2.5 km (1.6 mi) of burial, suggesting that 50 to 70% porosity units or 83 to 88% volume is lost by compactional and diagenetic processes. Cementation associated with burial is variable. It can take the form of precipitation of clays in pores (Figure 8D), cement overgrowths on grains by quartz, carbonate, or feldspar (Figure 7A), or as pore cement fill. As already discussed, abundant pores can be created in OM undergoing thermal maturation. Organic-matter pore development started with the onset of organic thermal maturation, but we found no linear correlation with increased maturation. This observation is based on an analysis of numerous Barnett Shale samples covering a range of R_o values (0.5–3.17% R_o). The

final pore network in a mudrock can be any combination of pore types.

SUMMARY AND CONCLUSIONS

A mudrock matrix-related pore classification is presented that can be used to categorize different pore types into three general classes: mineral matrix interP pores that developed between grains and crystals, mineral matrix intraP pores that are contained within a particle boundary, and intraP OM pores. Young shallow-buried muds contain only interP and intraP pores that are greatly diminished during burial and compaction. With deeper burial, OM pores develop during hydrocarbon thermal maturation, and intraP dissolution pores may develop by acidic fluid generated during decarboxylation of kerogen.

Mudrocks have a variety of pore networks that can be any combination of pore types. Development of the pore network depends on original mineralogy, fabric, and texture, which can vary at the millimeter lamination level. The OM content and type are important factors in the development and abundance of OM pores. Pores of all types appear to be able to stay open into the deep subsurface (>15,000 ft [>4570 m]).

The practical function of this pore classification is its application in characterizing pore networks in different rock types for reservoir characterization. Pore-type categories were developed to be relatively simple and objective while carrying some implications for permeability. Interparticle and OM pores have been demonstrated to have generally better connectivity than intraP pores. The latter pores will provide storage and some permeability but will not have the same level of connectivity as the other pore types. This classification of pore types depends on imaging of pores at the SEM level. Multiple two-dimensional images are needed to characterize each rock type quantitatively for pore networks, and several 3-D image analyses are necessary to substantiate that the pores are connected and form an effective pore network.

The major goal of imaging is to quantify and capture the strong heterogeneity observed at the submillimeter scale in mudrocks. A database of

combining pore-network types with mudrock types might show that certain mudrock types produce similar pore networks. Characterization of each mudrock type relative to its R_o level would also be essential.

The mudrock matrix-related pore classification presented here offers a simple but robust system for categorizing pores on the basis of their relationships with grains. Although pore types vary widely in origin, shape, and size, all pores can be assigned to one of the three categories defined here by visual examination at the SEM scale. Because the interrelationships between grains and pores that form the basis for this classification scheme relate directly to permeability, grouping of pores using this system may be a future aid in modeling and predicting reservoir quality relative to porosity and permeability. However, much more research and data collection are needed from a broad variety of pore networks from different mineral compositions and at different levels of maturity. These data need to be related to measured porosity and permeability analyses. We must also more fully understand the evolution of pore networks relative to increases in time, temperature, and pressure before reliable reservoir-quality prediction can be possible. Another application might be using this pore classification for defining general nanopore to micropore network types that can then be modeled for hydrocarbon flow. The types of pores within the network are a major controlling factor for storage, permeability, and wettability.

REFERENCES CITED

- Ambrose, R. J., R. C. Hartman, M. Diaz-Campos, I. Y. Akkutlu, and C. H. Sondergeld, 2010, New pore-scale considerations for shale gas in place calculations: Society of Petroleum Engineers Unconventional Gas Conference, Pittsburgh, Pennsylvania, February 23–25, 2010, SPE Paper 131772, 17 p.
- Boles, J. R., and S. G. Franks, 1979, Clay diagenesis in Wilcox sandstones of southwest Texas: Implication of smectite diagenesis on sandstone cementation: *Journal of Sedimentary Research*, v. 49, p. 55–70.
- Bridge, J. S., and R. V. Demicco, 2008, *Earth surface processes, landforms and sediment deposits*: New York, Cambridge University Press, 830 p.
- Chalmers, G., R. M. Bustin, and I. Powers, 2009, A pore by any other name would be as small: The importance of meso- and microporosity in shale gas capacity (abs.): AAPG Search and Discovery article 90090, 1 p.: <http://www.searchanddiscovery.com/abstracts/html/2009/annual/abstracts/chalmers.htm> (accessed March 14, 2011).
- Choquette, P. W., and L. C. Pray, 1970, Geologic nomenclature and classification of porosity in sedimentary carbonates: AAPG Bulletin, v. 54, p. 207–244.
- Clarke, R., 2007, Basin focus: Maverick Basin: *Oil and Gas Investor*, v. 27, p. 87–90.
- Curtis, M. E., R. J. Ambrose, C. H. Sondergeld, and C. S. Rai, 2010, Structural characterization of gas shales on the micro- and nano-scales: Canadian Unconventional Resources and International Petroleum Conference, Calgary, Alberta, Canada, October 19–21, 2010, SPE Paper 137693, 15 p.
- Davies, D. K., W. R. Bryant, R. K. Vessell, and P. J. Burkett, 1991, Porosities, permeabilities and microfabrics of Devonian shales, in R. H. Bennett, W. R. Bryant, and M. H. Hulbert, eds., *Microstructure of fine-grained sediments: From mud to shale*: New York, Springer-Verlag, p. 109–119.
- Dawson, W., and W. R. Almon, 2002, Top seal potential of Tertiary deep-water shales, Gulf of Mexico: *Gulf Coast Association of Geological Societies Transactions*, v. 52, p. 167–176.
- Day-Stirrat, R. J., S. P. Dutton, K. L. Milliken, R. G. Loucks, A. C. Aplin, S. Hillier, and B. E. van der Pluijm, 2010a, Fabric anisotropy induced by primary depositional variations in the silt: Clay ratio in two fine-grained slope fan complexes: Texas Gulf Coast and northern North Sea: *Sedimentary Geology*, v. 226, p. 42–53, doi:10.1016/j.sedgeo.2010.02.007.
- Day-Stirrat, R. J., P. B. Flemings, A. C. Aplin, and A. M. Schleicher, 2010b, The fabric and compaction of mudstones in the Gulf of Mexico (abs.): American Geophysical Union Fall Meeting, San Francisco, December 13–17, 2010, Abstract H43A-1213, 1 p.
- Day-Stirrat, R. J., K. Milliken, S. P. Dutton, R. G. Loucks, S. Hillier, A. C. Aplin, and A. M. Schleicher, 2010c, Open-system chemical behavior in deep Wilcox Group mudstones, Texas Gulf Coast, U.S.A.: *Marine and Petroleum Geology*, v. 27, p. 1804–1818, doi:10.1016/j.marpetgeo.2010.08.006.
- Desbois, G., J. L. Urai, and P. A. Kukla, 2009, Morphology of the pore space in claystones—Evidence from BIB/FIB ion beam sectioning and cryo-SEM observations: *Earth*, v. 4, p. 15–22, doi:10.1051/epjconf/2010062205.
- Dewhurst, D. N., Y. Yang, and A. C. Aplin, 1999, Permeability and fluid flow in natural mudstones, in A. C. Aplin, A. J. Fleet, and J. H. S., Macquaker, eds., *Muds and mudstones: Physical and fluid flow properties*: Geological Society (London) Special Publication 158, p. 23–43.
- Dewhurst, D. N., R. M. Jones, and M. D. Raven, 2002, Microstructural and petrophysical characterization of Muderong Shale: Application to top seal risk: *Petroleum Geoscience*, v. 8, p. 371–383, doi:10.1144/petgeo.8.4.371.
- Diaz, E., C. Sisk, and A. Nur, 2010, Quantifying and linking

- shale properties at a variable scale: 44th U.S. Rock Mechanics Symposium and 5th U.S.-Canada Rock Mechanics Symposium, Salt Lake City, Utah, June 27–30, 2010, American Rock Mechanics Association Paper 10-272, 3 p.
- Dow, W. G., 1977, Kerogen studies and geological interpretations: *Journal of Geochemical Exploration*, v. 7, p. 79–99, doi:[10.1016/0375-6742\(77\)90078-4](https://doi.org/10.1016/0375-6742(77)90078-4).
- Dutton, S. P., and R. G. Loucks, 2010, Diagenetic controls on evolution of porosity and permeability in lower Tertiary Wilcox sandstones from shallow to ultradeep (200–6700 m) burial, Gulf of Mexico Basin, U.S.A.: *Marine and Petroleum Geology*, v. 27, p. 69–81, doi:[10.1016/j.marpetgeo.2009.08.008](https://doi.org/10.1016/j.marpetgeo.2009.08.008).
- Eichhubl, P., and J. R. Boles, 1998, Vein formation in relation to burial diagenesis in the Miocene Monterey Formation, Arroyo Burro Beach, Santa Barbara, California, in P. Eichhubl, ed., *Diagenesis, deformation, and fluid flow in the Miocene Monterey Formation: Pacific Section SEPM Special Publication 83*, p. 15–36.
- Föllmi, K. B., 1996, The phosphorus cycle, phosphogenesis and marine phosphate-rich deposits: *Earth-Science Reviews*, v. 40, p. 55–124, doi:[10.1016/0012-8252\(95\)00049-6](https://doi.org/10.1016/0012-8252(95)00049-6).
- Fruehn, J., E. S. White, and T. A. Minshull, 1997, Internal deformation and compaction of the Makran accretionary wedge: *Terra Nova*, v. 9, p. 101–104.
- Gale, J. F. W., and J. Holder, 2010, Natural fractures in some U.S. shales and their importance for gas production: *Petroleum Geology Conference Series 7*, p. 1131–1140.
- Gale, J. F. W., R. M. Reed, and J. Holder, 2007, Natural fractures in the Barnett Shale and their importance for hydraulic fracture treatments: *AAPG Bulletin*, v. 91, p. 603–622, doi:[10.1306/11010606061](https://doi.org/10.1306/11010606061).
- Hayes, J. B., 1991, Porosity evolution of sandstones related to vitrinite reflectance: *Organic Geochemistry*, v. 17, p. 117–129.
- Hildenbrand, A., and J. L. Urai, 2003, Investigation of the morphology of pore space in mudstones: First results: *Marine and Petroleum Geology*, v. 20, p. 1185–1200.
- Hover, V. C., D. R. Peacor, and L. M. Walter, 1996, STEM/AEM evidence for preservation of burial diagenetic fabrics in Devonian shales: *Journal of Sedimentary Research*, v. 66, p. 519–530, doi:[10.1306/D4268397-2B26-11D7-8648000102C1865D](https://doi.org/10.1306/D4268397-2B26-11D7-8648000102C1865D).
- Jarvie, D. M., R. J. Hill, T. E. Ruble, and E. M. Pollastro, 2007, Unconventional shale-gas systems: The Mississippian Barnett Shale of north-central Texas as one model for thermogenic shale-gas assessment: *AAPG Bulletin*, v. 91, p. 475–499, doi:[10.1306/121906060608](https://doi.org/10.1306/121906060608).
- Javadpour, F., 2009, Nanopores and apparent permeability of gas flow in mudrocks (shales and siltstone): *Journal of Canadian Petroleum Technology*, v. 48, p. 16–21.
- Kanitpanyacharoen, W., W. Hans-Rudolf, F. Kets, C. Lehr, and R. Wirth, 2011, Texture and anisotropy analysis of Qusaiba shales: *Geophysical Prospecting*, v. 59, p. 536–556.
- Kastner, M., J. B. Keene, and J. M. Gieskes, 1977, Diagenesis of siliceous oozes: I. Chemical controls on the rate of opal-A to opal-CT transformation—An experimental study: *Geochimica et Cosmochimica Acta*, v. 41, p. 1041–1059.
- Kwon, O., A. K. Kronenberg, A. F. Gangi, B. Johnson, and B. E. Herbert, 2004, Permeability of illite-bearing shale: I. Anisotropy and effects of clay content and loading: *Journal of Geophysical Research*, v. 109, no. B10205, 19 p., doi:[10.1029/2004JB003052](https://doi.org/10.1029/2004JB003052).
- Land, L. S., and K. L. Milliken, 2000, Regional loss of SiO₂ and CaCO₃ and gain of K₂O during burial diagenesis of Gulf Coast mudrocks, U.S.A., in R. H. Worden and S. Morad, eds., *Quartz cementation in sandstones*: Oxford, Blackwell Science, International Association of Sedimentologists Special Publication 29, p. 183–198.
- Loucks, R. G., and S. C. Ruppel, 2007, Mississippian Barnett Shale: Lithofacies and depositional setting of a deep-water shale-gas succession in the Fort Worth Basin, Texas: *AAPG Bulletin*, v. 91, p. 579–601, doi:[10.1306/11020606059](https://doi.org/10.1306/11020606059).
- Loucks, R. G., R. M. Reed, S. C. Ruppel, and D. M. Jarvie, 2009, Morphology, genesis, and distribution of nanometer-scale pores in siliceous mudstones of the Mississippian Barnett Shale: *Journal of Sedimentary Research*, v. 79, p. 848–861, doi:[10.2110/jsr.2009.092](https://doi.org/10.2110/jsr.2009.092).
- Loucks, R. G., R. M. Reed, S. C. Ruppel, S. C., and U. Hammes, 2010, Preliminary classification of matrix pores in mudrocks: Gulf Coast Association of Geological Societies Transactions, v. 60, p. 435–441.
- Lu, J., K. L. Milliken, R. M. Reed, and S. Hovorka, 2011, Diagenesis and sealing capacity of the middle Tuscaloosa mudstone at the Cranfield carbon dioxide injection site, Mississippi, U.S.A.: *Environmental Geosciences*, v. 18, p. 35–53, doi:[10.1306/eg.09091010015](https://doi.org/10.1306/eg.09091010015).
- Lucia, F. J., 1999, *Carbonate reservoir characterization*: New York, Springer-Verlag, 226 p.
- MacGowan, D. B., and R. C. Surdam, 1990, Carboxylic acid anions in formation waters, San Joaquin Basin and Louisiana Gulf Coast, U.S.A.: Implications for clastic diagenesis: *Applied Geochemistry*, v. 5, p. 687–701.
- Matheny, R. K., and L. P. Knauth, 1993, New isotopic temperature estimates for early silica diagenesis in bedded cherts: *Geology*, v. 21, p. 519–522, doi:[10.1130/0091-7613\(1993\)021<0519:NITEFE>2.3.CO;2](https://doi.org/10.1130/0091-7613(1993)021<0519:NITEFE>2.3.CO;2).
- McCreesh, C. A., R. Erlich, and S. J. Crabtree, 1991, Petrography and reservoir physics II: Relating thin section porosity to capillary pressure, the association between pore types and throat size: *AAPG Bulletin*, v. 75, p. 1563–1578.
- Milliken, K. L., and R. M. Reed, 2010, Multiple causes of diagenetic fabric anisotropy in weakly consolidated mud, Nankai accretionary prism, IOPD Expedition 316: *Journal of Structural Geology*, v. 32, p. 1887–1898, doi:[10.1016/j.jsg.2010.03.008](https://doi.org/10.1016/j.jsg.2010.03.008).
- Milner, M., R. McLin, and J. Petriello, 2010, Imaging texture and porosity in mudstones and shales: Comparison of secondary and ion milled backscatter SEM methods: Canadian Unconventional Resources and International Petroleum Conference, Calgary, Alberta, Canada, October 19–21, 2010, Canadian Society for Unconventional Gas/Society of Petroleum Engineers Paper 138975, 10 p.
- Passey, Q. R., K. M. Bohacs, W. L. Esch, R. Klimentidis, and S. Sinha, 2010, From oil-prone source rock to gas-producing

- shale reservoir: Geologic and petrophysical characterization of unconventional shale-gas reservoirs: International Oil and Gas Conference and Exhibition, Beijing, China, June 8–10, 2010, SPE Paper 131350, 29 p.
- Pitman, J. K., L. C. Price, and J. A. LeFever, 2001, Diagenesis and fracture development in the Bakken Formation, Williston Basin: Implications for reservoir quality in the middle member: U.S. Geological Survey Professional Paper 1653, 19 p.
- Pittman, E. D., 1979, Porosity, diagenesis and productive capability of sandstone reservoirs, in P. A. Scholle and P. R. Schluger, eds., *Aspects of diagenesis*: SEPM Special Publication 26, p. 159–173.
- Pittman, E. D., 1992, Artifact porosity in thin sections of sandstones: *Journal of Sedimentary Research*, v. 62, p. 734–737.
- Pytte, A. M., and R. C. Reynolds, 1988, The thermal transformation of smectite to illite, in N. D. Naeser and T. H. McCulloh, eds., *Thermal histories of sedimentary basins*: New York, Springer-Verlag, p. 133–140.
- Raiswell, R., 1976, The microbiological formation of carbonate concretions in the Upper Lias of NE England: *Chemical Geology*, v. 18, p. 227–244.
- Reed, R. M., and R. G. Loucks, 2007, Imaging nanoscale pores in the Mississippian Barnett Shale of the northern Fort Worth Basin (abs.): AAPG Annual Convention Abstracts, v. 16, p. 115.
- Rieke, H. H., and G. V. Chilingarian, 1974, *Compaction of argillaceous sediments: Developments in sedimentology*: Amsterdam, Elsevier, v. 16, 424 p.
- Ross, D. J. K., and R. M. Bustin, 2009, The importance of shale composition and pore structure upon storage potential of shale gas reservoirs: *Marine and Petroleum Geology*, v. 26, p. 916–927, doi:10.1016/j.marpetgeo.2008.06.004.
- Rouquerol, J., D. Avnir, C. W. Fairbridge, D. H. Everett, J. H. Haynes, N. Pernicone, J. D. F. Sing, and K. K. Unger, 1994, Recommendations for the characterization of porous solids: *Pure and Applied Chemistry*, v. 66, p. 1739–1758, doi:10.1351/pac199466081739.
- Ruppel, S. C., and R. G. Loucks, 2008, Black mudrocks: Lessons and questions from the Mississippian Barnett Shale in the southern mid-continent: *The Sedimentary Record*, v. 6, p. 4–8.
- Schieber, J., 2010, Common themes in the formation and preservation of porosity in shales and mudstones: Illustrated with examples across the Phanerozoic: Society of Petroleum Engineers Unconventional Gas Conference, Pittsburgh, Pennsylvania, February 23–25, 2010, SPE Paper 132370, 12 p.
- Sisk, C., D. Diaz, J. Walls, A. Grader, and M. Suhrer, 2010, 3-D visualization and classification of pore structure and pore filling in gas shales: Society of Petroleum Engineers Annual Technical Conference and Exhibition, Florence, Italy, September 19–22, 2010, SPE Paper 134582, 4 p.
- Slatt, E. M., and N. R. O'Neal, 2011, Pore types in the Barnett and Woodford gas shale: Contribution to understanding gas storage and migration pathways in fine-grained rocks (abs.): AAPG Annual Convention Abstracts, v. 20, p. 167.
- Sondergeld, C. H., R. J. Ambrose, C. S. Rai, and J. Moncrieff, 2010, Microstructural studies of gas shales: Society of Petroleum Engineers Unconventional Gas Conference, Pittsburgh, Pennsylvania, February 23–25, 2010, SPE Paper 131771, 17 p.
- Surdam, R. C., D. B. MacGowan, and T. L. Dunn, 1991, Predictive models for sandstone diagenesis: *Organic Geochemistry*, v. 17, p. 242–253.
- Tomutsa, L., D. Silin, and V. Radmilovic, 2007, Analysis of chalk petrophysical properties by means of submicron-scale pore imaging and modeling: Society of Petroleum Engineers Reservoir Evaluation and Engineering, v. 10, p. 285–293.
- TXCO Resources, 2009, The emerging resource company, TXCO Resources: Howard Weil 37th Annual Energy Conference, New Orleans, March 22–29, 2009, 35 p.: <http://www.scribd.com/doc/20128412/The-Emerging-Resource-Company> (accessed March 25, 2011).
- Van Sickel, W. A., M. A. Kominz, K. G. Miller, and J. V. Browning, 2004, Late Cretaceous and Cenozoic sea level estimates: Backstripping analysis of borehole data, onshore New Jersey: *Basin Research*, v. 16, p. 451–465, doi:10.1111/j.1365-2117.2004.00242.x.
- Weeks, L. G., 1957, Origin of carbonate concretions in shales, Magdalena Valley, Colombia: *Geological Society of America Bulletin*, v. 88, p. 95–102, doi:10.1130/0016-7606(1957)68[95:OOCIS]2.0.CO;2.
- Wilkin, R. T., H. L. Barnes, and S. L. Brantley, 1996, The size distribution of framboidal pyrite in modern sediments: An indicator of redox conditions: *Geochimica et Cosmochimica Acta*, v. 60, p. 3897–3912, doi:10.1016/0016-7037(96)00209-8.
- Wilkin, R. T., M. A. Arthur, and W. E. Dean, 1997, History of water column anoxia in the Black Sea indicated by pyrite framboids size distributions: *Earth and Planetary Science Letters*, v. 148, p. 517–525, doi:10.1016/S0012-821X(97)00053-8.
- Williams, L. A., and D. A. Crerar, 1985, Silica diagenesis: II. General mechanisms: *Journal of Sedimentary Petrology*, v. 55, p. 312–321, doi:10.1306/212F86B1-2B24-11D7-8648000102C1865D.